DEVELOPMENT OF A COMPOSITIONAL RESERVOIR SIMULATOR FOR ASPHALTENE PRECIPITATION BASED ON A THERMODYNAMICALLY CONSISTENT MODEL

A Thesis

by

KARIN GABRIELA GONZALEZ ABAD

Submitted to the Office of Graduate Studies of
Texas A&M University
in partial fulfillment of the requirements for the degree of

MASTER OF SCIENCE

Chair of Committee,	Maria A. Barrufet
Co-Chair of Committee,	Hadi Nasrabadi
Committee Member,	Hisham Nasr-El-Din
Head of Department,	Daniel Hill

August 2013

Major Subject: Petroleum Engineering

ABSTRACT

A rigorous three-phase asphaltene precipitation model was implemented into a compositional reservoir simulator to represent and estimate the reduction of porosity and permeability responsible for productivity impairment. Previous modeling techniques were computationally inefficient, showed thermodynamic inconsistencies, or required special laboratory experiments to characterize the fluid.

The approach developed in this study uses a cubic equation of state to solve for vapor/liquid/liquid equilibrium (VLLE), where asphaltene is the denser liquid phase. Precipitation from the liquid mixture occurs as its solubility is reduced either by changes in pressure (natural depletion), or composition (i.e. mixing resulting from gas injection). The dynamic relationship between phase composition, pressure, and porosity/permeability is modeled with a finite differences reservoir simulator and solved using an implicit-pressure, explicit-saturations and explicit-compositions (IMPESC) direct sequential method.

The robustness of this model is validated by the ability to reproduce experimental asphaltene precipitation data while predicting the expected phase behavior envelope and response to key thermodynamic variables (i.e. type of components and composition, pressure and, temperature).

The three-phase VLLE flash provides superior thermodynamic predictions compared to existing commercial techniques. Computer performance analysis showed that the model has a comparable cost to existing asphaltene precipitation models, taking only 1.1 more time to calculate but requiring fewer tunable parameters. The VLLE flash was in average 4.47 times slower compared to a conventional two-phase vapor/liquid flash.

This model has the speed of a flash calculation while maintaining thermodynamic consistency, enabling efficient optimization of reservoir development strategies to mitigate the detrimental effects of asphaltene precipitation on productivity.

ACKNOWLEDGMENTS

I would like to offer my deepest gratitude to the committee members who have supported me throughout this research with their expertise and precious time. Special thanks to Dr. Maria Barrufet for her invaluable mentoring and immense enthusiasm during the MS studies. Without her guidance and persistent help, this work would not have been possible. My co-advisor, Dr. Hadi Nasrabadi, for his insightful and discerning comments on reservoir simulation techniques. Dr. Hisham Nasr-El-Din, for conveying his high research standards and innovative ideas.

In addition, my appreciations to the professors of the petroleum engineering department at Texas A&M University who have deepened my keen interest in research through classes, seminars, and discussions.

I wish to thank my family for their unconditional support and confidence throughout my studies. Most of all, my beloved husband Ernesto whose continuous support, encouragement, and advices made graduate school an extraordinary experience. Thank you.

Finally, I gratefully acknowledge Qatar National Research Fund for supporting this research under grant NPRP 09-1050-2-405.

NOMENCLATURE

A	Flow cross-sectional area
c_f	Rock compressibility
f_α	Phase fraction (with superscript $\alpha = v, l, s$)
f_i	Fugacity of pure component (with subscripts i, j)
$\widehat{f_i}$	Fugacity of component in a mixture
G_t	Total Gibbs energy
h	Depth
k	Permeability
K	Vapor/liquid equilibrium ratio of component
kr	Relative permeability
l	Liquid
L	Block length
Mw	Molecular weight
n	Number of moles
Nc	Number of component
Np	Number of phases
p	Pressure
P_c	Critical pressure
P_{pc}	Pseudo critical pressure
P_r	Reduced pressure
p_{wf}	Bottomhole flowing pressure
pc_{VL}	Capillary pressure vapor-liquid
q	Molar rate
Q	Volumetric rate
R	Universal gas constant
s	Solid

t	Time
T	Temperature
T_c	Critical temperature
T_{pc}	Pseudo critical temperature
T_r	Reduced temperature
V	Volume
v	Vapor
$\overline{V_i}$	Partial molar volume of component i
V_m	Molar volume
V_p	Pore volume
Vc	Critical volume
$wt\%$	Weight fraction
x_i	Molar fraction of component i in the liquid phase
y_i	Molar fraction of component i in the vapor phase
z_i	Molar fraction of component i in the mixture
Z	Compressibility factor

Greek Symbols

α	Permeability reduction parameter (in Chapters V and VI)
ϵ	Convergence criteria
ζ	Viscosity parameter
κ	Binary interaction coefficient
μ	Chemical potential (in Chapter III)
μ	Viscosity (in Chapters V and VI)
ρ_m	Molar density
ϕ	Porosity
Φ	Flow potential

φ	Fugacity coefficient of a pure component
$\widehat{\varphi}$	Fugacity coefficient of component in a mixture
ω	Acentric factor

Superscripts

k	Iteration
l	Liquid phase
n	Time level
s	Solid phase
v	Vapor phase
ℓ	Phase

Subscripts

$asph$	Asphaltene pseudo-component
B	Bottom block
C	Central block
E	East block
i	Component index
j	Component index
l	Liquid phase
N	North block
s	Solid phase
S	South block
T	Top block
v	Vapor phase
W	West block
ℓ	Phase

Abbreviations

ADE	Asphaltene deposition envelope
AOP	Asphaltene offset pressure
BIC	binary interaction coefficient
EOS	Equation of state
IMPESC	Implicit-pressure, explicit-composition, and explicit-saturations method
MVNR	Minimum-variable Newton-Raphson
PC-SAFT	Perturbed chain form of the statistical associating fluid theory
PVT	Pressure-volume-temperature
SRK	Soave-Redlich-Kwong
VLE	Vapor-liquid equilibrium
VLLE	Vapor-liquid-liquid equilibrium
WI	Well index

TABLE OF CONTENTS

Page

Page

LIST OF TABLES

TABLE Page

LIST OF FIGURES

FIGURE Page

FIGURE Page

FIGURE Page

CHAPTER I
INTRODUCTION

Asphaltene is a highly viscous hydrocarbon fraction that can precipitate and deposit along the production system, plugging the reservoir pore throat, wellbore, flowlines, or surface facilities. This results in significant reduction of productivity and high-cost remedial operations (Leontaritis and Ali Mansoori, 1988). Precipitation from live oils can be mitigated by properly designing and optimizing a reservoir development program. This requires full-scale reservoir modeling and detailed understanding of the conditions at which asphaltene deposits.

Precipitation can be triggered by changes in pressure (depletion by production), temperature (heat transfer along the production path), or composition (either from gas cycling, enhanced oil recovery with CO_2, or diffusion in strongly compositional reservoirs). The complexity of asphaltene molecules has resulted in multiple theories describing its behavior within an oil mixture. Li and Firoozabadi (2010a,b) classified them as lyophobic, where asphaltene is considered insoluble in the oil but it is stabilized by resins; and lyophilic, where asphaltene precipitates as a result of the reduction of the solvent power of the hydrocarbon fluid. The latter has had better acceptance in numerical simulation due to its flexibility to adapt to the framework of existing software.

In a reservoir simulator, the phase behavior model determines compositions, saturations, and pressure distribution. For solid precipitation cases, asphaltene saturation also dictates porosity and permeability variation, which consequently affects the pressure solution. These tightly-coupled and highly non-linear relations present an important mathematical challenge when modeling this type of reservoirs.

Current commercial simulators do not represent the physical phenomena of asphaltene. The main problems are observed in the precipitation model and its prediction capabilities, the mechanisms describing deposition and transport of asphaltene within the rock, and their effect on permeability and other dynamic variables that cause formation damage. In this research, we focused on implementing a fluid model based on the lyophilic theory as proposed by Pedersen and Christensen (2006), where the liquid-dense fraction is assumed to be pure asphaltene (pseudo-component) and the equilibrium state is calculated using Peng-Robinson EOS for a three-phase system. This approach offers the robustness and speed of a flash calculation while maintaining thermodynamic consistency.

The 3D finite difference simulator was developed in a mass balance form, and it accounts for the reduction of porosity and permeability as a function of asphaltene precipitation. Because of the strong and non-linear relation between pressures and porosity/permebility, the solution was achieved using implicit-pressure, explicit-composition, and explicit-saturations method (IMPESC) based on direct sequential method as suggested by Acs et al. (1985). The reservoir simulator was implemented in MATLAB®.

1.1 Objectives

The main objective of this research was to propose and develop a reservoir simulation model capable of predicting asphaltene precipitation. In order to accomplish this goal, we completed the following specific tasks:

1. Developed and implemented an algorithm to estimate asphaltene precipitation based on a three-phase flash vapor/liquid/liquid-dense equilibrium using Peng-Robinson EOS.

2. Validated the phase behavior model against data published in the literature.

3. Implemented and tested the three-phase flash model into a 3D compositional reservoir simulator solved with IMPESC.

1.2 Description of the chapters

Chapter I defines the general problem of this research, including relevance, approach, and objectives accomplished.

Chapter II presents a literature review, starting with a description of asphaltene molecules and current thermodynamic models available for predicting its behavior. We also describe the generalities of full-field reservoir simulators and the mathematical formulations for fully compositional cases. We analyzed the asphaltene precipitation modules implemented in current commercial simulators and identified their applicability and limitations.

Chapter III shows the equations describing phase behavior of asphaltene. It includes most commonly used equations of the state (EOS), theory of phase equilibrium, and development of a three-phase flash algorithm for predicting asphaltene precipitation based on successive substitution.

In Chapter IV, we validated and analyzed the fluid model by comparing with experimental data previously published by Burke et al. (1990), with cases based on changes of pressure and solvent injection. In addition, we performed several sensitivity studies to understand the effect of asphaltene characterization in the overall precipitation. We also analyzed the computational efficiency by comparing the CPU running time versus a conventional two-phase flash.

Chapter V describes the mathematical formulation of a 3D numerical reservoir simulator that accounts for asphaltene precipitation. It includes the derivation of transport equations for a finite-difference, three-phase (vapor, liquid, and asphaltene), and fully compositional model. This chapter also shows the assumptions taken and the solution method (IMPESC) used to reach the solution.

Chapter VI shows the application of the simulator for predicting asphaltene precipitation within the reservoir. It includes homogeneous and heterogeneous cases to analyze the mechanisms involved in solid precipitation and test the robustness and stability of the algorithm.

Finally, Chapter VII states the conclusions and recommendations for future research.

CHAPTER II
LITERATURE REVIEW

2.1 Asphaltene description

Petroleum reservoir fluids are naturally existing mixtures composed by hundreds or thousands of hydrocarbon and non-hydrocarbon components. Their composition can be classified depending on the component class into four large groups as defined by Pedersen and Christensen (2006).

- Paraffins or alkanes: Chains of hydrocarbon segments (CH, CH_2, or CH_3) connected by single bonds.
- Naphthenes: Cyclic structures built of the same type of hydrocarbon segments as the paraffins.
- Aromatics: Structures with one or more cyclic structures connected by aromatic double bonds.
- Asphaltenes and resins: Large and highly concentrated molecules composed mainly by hydrogen and carbon with some heteroatoms (e.g. sulfur, oxygen, nitrogen) and metals. Asphaltenes are defined as the fraction practically insoluble in n-pentane and n-heptane but soluble in benzene and toluene at room temperature. Resins are defined as the fraction practically insoluble in liquid propane at room temperature.

The definition of asphaltenes and resins is based on a solubility concept; therefore their molecules cannot be physically and chemically described as pure. Their general structure is very similar because they are both formed by oxidation of polycyclic aromatic hydrocarbons (McCain, 1990). The main difference between them is their solubility properties in solvents.

Measuring the molecular weight of asphaltene represents a big challenge. Hunt et al. (1997) observed that asphaltene forms molecular aggregates depending on factors such as polarity of the solvent, temperature, concentration, and others. For this reason, reported asphaltene molecular weights range greatly, from 800 to 50,000 $lb/lb-mol$ or even higher (Firoozabadi, 1999).

The general mechanistic behavior of asphaltene can be described by the asphaltene deposition envelope (ADE), a concept originally proposed by Leontaritis (1996) and depicted in **Fig. 2.1**. It represents the relationship between pressure and temperature, where asphaltene precipitation is defined by two curves: ADE upper boundary, above which asphaltene does not precipitate, and ADE lower boundary, below which asphaltene does not precipitate.

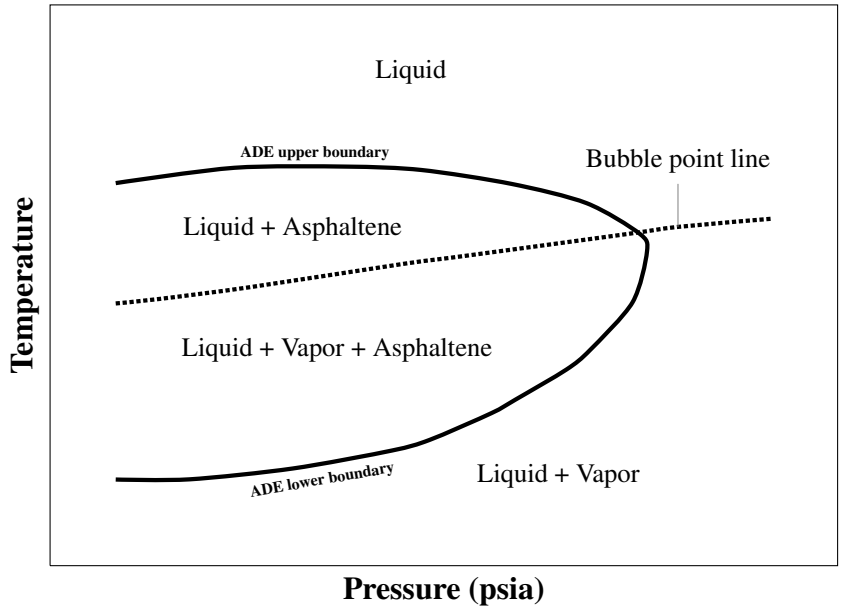

Fig. 2.1—Typical p-T asphaltene precipitation envelope as proposed by Leontaritis (1996) where precipitation occurs only within the region defined between the ADE upper boundary and the ADE lower boundary [adapted from Leontaritis (1996)].

For a reservoir with fixed-liquid composition at initial reservoir pressure and temperature above the upper ADE boundary, no asphaltene precipitates from the mixture. As pressure decreases, the fluid will cross the ADE upper boundary and the first asphaltene molecules will precipitate as a solid phase. This occurs as the solubility of asphaltenes in paraffins decreases with pressure.

The largest asphaltene precipitation will typically occur very close to the bubble point pressure (Pedersen and Christensen, 2006), where the fluid has the highest concentration of dissolved gas (C_1, C_2, etc.), which is bad solvent for asphaltene. At lower pressure, gas breaks out of solution reducing the gas concentration in the liquid fraction. This makes asphaltene more soluble in the liquid and asphaltene slowly re-dissolves in the mixture. Once the system conditions reach the lower ADE boundary, no asphaltene precipitates from the solution.

2.2 Phase behavior of asphaltenes

The complexity of asphaltene molecules has resulted in multiple theories describing the precipitation process from live oils. Li and Firoozabadi (2010a,b) classified the theoretical approaches into two main categories depending on the mechanisms of precipitation and stabilization: lyophobic and lyophilic.

2.2.1 Lyophobic theory

Lyophobic models assume asphaltene to be insoluble in the oil mixture but they can be stabilized by resins adsorbed on their surface. Asphaltene precipitation occurs as a result of resin desorption from the asphaltene's surface (**Fig. 2.2**). Civan (2000) suggests that the crude oil can be divided into two parts: high boiling-point polar asphaltic components, and the rest of the crude oil which acts as a solvent for maintaining the asphaltene molecules in suspension. The resins help asphaltene to disperse in oil as a suspension by means of

hydrogen-bonding and irreversible acid/base reactions of asphaltene and resin molecules. This theory includes the colloidal model proposed by Leontaritis and Mansoori (1987) and the micellization model proposed by Pan and Firoozabadi (2000).

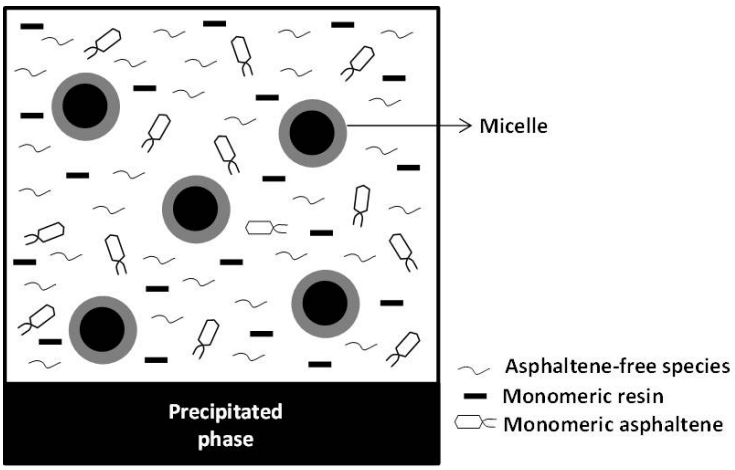

Fig. 2.2—Physical description of asphaltene precipitation and stabilization according to the lyophobic theory. Asphaltene micelles have spherical shape surrounded by resins that help its stabilization in the fluid mixture [adapted from Firoozabadi (1999)]

2.2.2 Lyophilic theory

The lyophilic theory assumes that asphaltene precipitates when the hydrocarbon fluid reduces its solvent power. This can be described as a conventional liquid/liquid or liquid/solid equilibrium, reached when all molecules have the same temperature, pressure, and chemical potential, whether they are present in the solid, liquid, or gas phase. The following five models use this approach for representing asphaltene precipitation.

Solubility theory based on Flory-Huggins

The solubility theory is based on Flory-Huggins's approach for modeling polymer solutions. Asphaltene precipitation depends on how much the solubility parameters of the liquid phase deviate from the asphaltene solubility parameter. The closer the solubility pa-

rameters are to each other, the higher the amount of asphaltene that will remain in solution (Hirschberg et al., 1984; Wang, 2000).

The fluid composition from Flory-Huggins is represented only by two or three components. The conditions for vapor/liquid equilibrium use cubic EOS, assuming that asphaltene precipitation does not affect the equilibrium. This model is fast and simple to apply, but it lacks proper representation for volatile oils or gas injection cases where there strong composition changes are observed.

Perturbed chain form of the statistical associating fluid theory (PC-SAFT)

The perturbed chain form of the statistical associating fluid theory (PC-SAFT) assumes that molecular size and nonpolar van der Waals interactions dominate asphaltene phase behavior (Gonzalez et al., 2007; Vargas et al., 2009). This model describes the molecules as a chain of bonded spherical segments, using the number of segments and the van der Waals attraction forces between segments to model the fluid behavior. This theory has the capacity to predict the effect of association between molecules of different sizes and accurate calculate densities of well-defined components (CO_2, CH_3OH, etc.) commonly used in downstream analyses. However, its mathematical complexity significantly increases CPU consumption particularly in multi-phase flow, and it requires additional laboratory experiments to characterize the plus fraction (Yan et al., 2011).

Cubic plus association equation of state (CPA-EOS)

The cubic plus association EOS combines a conventional cubic EOS and the association term derived from statistical associating fluid theory (Kontogeorgis et al., 2006; Li and Firoozabadi, 2010a,b). All components are characterized with critical properties and acentric factors, similar to a conventional EOS, and they can exist in all phases (liquid, vapor, and solid). The heavier component is further divided into resins, a nonprecipitating

fraction, and asphaltenes, a precipitating fraction.

The modified equation of state consists of two contributing parts: physical and association. The physical part represents the interaction of short-range repulsion and attractions forces of non-association molecules. This part is represented by a conventional cubic EOS, like Peng-Robinson or Soave-Redlich-Kwong. On the other hand, the association part describes the polar/polar interaction of self-associating and cross-associating, this includes the asphaltene/resin interaction. The association term is derived from the thermodynamic perturbation theory used in PC-SAFT (Li and Firoozabadi, 2010a,b). This model has limitations similar to the ones observed in PC-SAFT, with additional computational times and requirements for better fluid description.

Cubic equation of state: vapor/liquid/solid equilibrium

The vapor/liquid/solid model is the most common approach currently used for reservoir simulation, where the precipitated asphaltene is assumed to be a pure solid. It has been implemented in several commercial and research reservoir simulators (Computer Modeling Group Ltd., 2011; Fazelipour, 2007). It requires to split the heaviest component into two fractions, a precipitating (asphaltene) and nonprecipitating (high molecular weight paraffin fraction). Both components have the same critical properties and acentric factor, but different interaction coefficient parameters. The precipitating component has larger binary interaction coefficient with the light components (C_1 - C_5) as described by Nghiem (1999).

The fugacity of the vapor and liquid phase are modeled using the conventional EOS, while the fugacity of the precipitated component is calculated as a solid using the model by Gupta (1986) and Thomas et al. (1992). The solid fugacity for isothermal conditions is calculated from Eq. 2.1, where f_s is the solid fugacity at p and T, f_s^* is the reference solid fugacity, p is the pressure, T is the temperature, R is the universal gas constant, and v_s is

the solid molar volume. This assumes constant properties for asphaltene, independent of pressure.

$$\ln f_s = \ln f_s^* + \frac{v_s(p - p^*)}{RT} \tag{2.1}$$

The solid model requires to explicitly defined a reference pressure, solid molar volume, and fugacity of solid at reference condition. These parameters can be obtained from laboratory experimental data, however, they are difficult to obtain. For practical reasons, the input solid fugacity is calculated with a two-phase flash EOS assuming the asphaltene precipitation pressure. At this point, the fugacity of the asphaltene is equal in the liquid and solid phase. The solid molar volume is estimated based on the solid molar volume of the entire liquid phase. The molar volume of the precipitated asphaltene is used for matching experimental data.

The input requirements result in lack of prediction capability, while the manual manipulation of thermodynamic parameters could result in inconsistencies when solving an equilibrium state.

Cubic equation of state: vapor/liquid/liquid-dense equilibrium

The cubic vapor/liquid/liquid-dense model proposed by Pedersen and Christensen (2006) performs a three-phase flash calculation, where the asphaltene phase is modeled as a liquid-dense phase in a conventional liquid/liquid equilibrium. To reduce the computational requirements of the multiphase flash vapor/liquid/liquid, the second liquid phase (asphaltene) can be represented as a pure component.

To characterize the asphaltene molecules, the plus fraction is split into precipitating (asphaltene) and nonprecipitating (solvent). Both fraction are defined as a pure components with unique, fixed, and known properties (critical temperature, critical pressure, and acen-

tric factor). Precipitation will be determined based on the stability of each phase modeled by a cubic EOS. The theory and equations are explained further in Chapter III.

This model is very robust and consistent with thermodynamic principles, while maintains the speed and applicability of a conventional flash calculation. In addition, it can be rapidly implemented and analyzed using fluid characterization based on current laboratory practices. Currently, this model is implemented in the commercial PVT simulation package PVTSim Calsep (2010). However, it has not been used in numerical reservoir simulators.

2.2.3 Selection of theory and model

Based on the simplicity and robustness of traditional cubic EOS, the lyophilic theory has had a greater acceptance in the industry for reservoir simulation. This approach is the most practical to model asphaltene precipitation from live oils as it can fully represent the phase behavior of the entire mixture using available characterization techniques.

From the models that use a cubic EOS, the dense-liquid model offers several advantages over the solid one. Both are three-phase flash, which are simple and fast calculations. However, the solid model requires additional input parameters and can result in thermodynamic inconsistencies by explicitly defining the solid molar volume. For this study, we used the cubic equations of state: vapor/liquid/liquid-dense equilibrium model.

2.3 Reservoir simulation of asphaltene precipitation

Reservoir simulation is an important tool for predicting and understanding the reservoir performance. In highly asphaltenic reservoirs, this method can be used to identify the conditions at which asphaltene precipitates, providing valuable information for field management. The following sections describe the models currently implemented in commercial

reservoir simulators and the mathematic formulation of compositional simulators as they can be applied for asphaltene precipitation.

2.3.1 Implementation in current reservoir simulators

Numerical modeling of asphaltene precipitation within the reservoir has become an important technique for flow assurance analyses. Existing compositional simulators have been adapted to represent asphaltene precipitation using cubic equations of state based on the lyophilic theory (Computer Modeling Group Ltd., 2011; Schlumberger, 2011). There are two main models commercially available for asphaltene precipitation: look-up table and liquid/vapor/solid equilibrium.

Precipitation by table look-up

The table look-up approach represents the asphaltene precipitation in a solubility-like model, where the asphaltene is assumed to be dissolved in the oil phase. The amount of asphaltene that precipitates, also referred as fines, is defined by the user as a look-up-table with respect to another variable (usually pressure or mole fraction of a specific component).

In this approach, asphaltene precipitation does not change the fluid composition and thus, it does not incorporates phase equilibrium. It only flags and limits the precipitation of a component that will contribute to the flocculation process (Yi et al., 2009). The flocculation model describes the process of aggregation of fines to form larger particles or flocs. This process is thermodynamically reversible; fines can aggregate to form flocs, and flocs can dissociate to form fines. This phenomenon is represented by a kinetic reaction.

Once the flocs are formed, they can deposit into the rocks following the approach proposed by Wang (2000), where the asphaltene flocs can be adsorbed on the rock, get plugged within the pore throat, or be flushed away by oil due its velocity (entrainment). The effect

of each mechanism is represented by user-defined parameters.

In the table look-up approach, asphaltene precipitation/flocculation is calculated independently from the phase behavior of the mixture, which is performed as a two-phase equilibrium. This a clear violation of thermodynamic equilibrium and material balance and does not represent consistently the equilibrium between the three existing phases.

Precipitation by liquid/vapor/solid equilibrium

The liquid/vapor/solid equilibrium approach uses the asphaltene precipitation model proposed by Nghiem and previously explained in this chapter. It represents asphaltene as a solid phase and uses the model by Gupta (1986) and Thomas et al. (1992) to calculate the phase fugacity. The dynamic interaction of the precipitated asphaltene within the reservoir is presented using Wang (2000) model.

2.3.2 Mathematic formulation of compositional simulators

For reservoirs with substantial mass transfer between phases, the fluid must be described as a set of components or pseudocomponents equilibrated thermodynamically along the entire system. This is particularly relevant in strongly compositional fluids (volatile oil or gas condensate) and in miscible gas injection processes.

The solution of a compositional reservoir simulator depends on constraints for mass balance, volume balance, sum of saturations to unity, and phase equilibrium of the components in each phase. The first approach to model compositional reservoirs was developed in the 1970s, followed by numerous models based on different formulations and matrix solution schemes. Based on the formulation of the equations, these methods can be divided into two types: mass balance and volume balance.

Mass balance type

The mass balance formulation uses the mass balance equation of each hydrocarbon component. It was first proposed by Fussell and Fussell (1979), who developed a compositional model based on Redlich-Kwong EOS where flow coefficients are solved explicitly, while compositions and pressure are treated as unknown at each time step. Fussell and Fussell proposed the solution of the equations using an iterative method called minimum-variable Newton-Raphson (MVNR) method, attempting to minimize the number of variables for which simultaneous iterations are required, while using the Newton-Raphson iterative method for the correction step.

Coats (1980) developed a fully-implicit, three-phase model using an EOS for calculating phase equilibrium and fluid properties. The implicit treatment of transmissibilities (depending of rock and fluid properties) removed the time-step limitation associated with models using explicit transmissibilities, but it also increased the amount of calculations required for every time step.

Nghiem et al. (1981) proposed a model solved with IMPESC. The formulation of the pressure equation was similar to a black-oil model, with a symmetric and diagonally dominant matrix that allowed the use of iterative methods. Mansoori (1982) observed that the model proposed by Nghiem et al. (1981) included approximations not valid for pressures across the bubblepoint of an oil reservoir or the dewpoint of a gas condensate and it could result in convergence problems.

Young and Stephenson (1983) presented a modification to Fussell and Fussell (1979) where they used the MVNR but reordered the equations and unknowns. It resulted in efficient computations and could incorporate fluid property correlations using a unified framework.

Volume balance type

The volume balance formulation is based on the concept that the pore space of the porous medium must be filled with the fluids that are present at any time and space. The total fluid is a function of pressure and composition. This method was introduced by Acs et al. (1985) using an IMPESC formulation.

Watts (1986) used Acs et al. volume equation and solved the pressure implicitly while solving the saturation using Spillette et al. (1973) semi-implicit approach.

2.3.3 Discussion and selection of mathematic formulation

To model asphaltene precipitation within the reservoir, we describe the fluid using a three-phase vapor/liquid/liquid-dense flash as previously analyzed. This practice guarantees a thermodynamic equilibrium of the system and a proper representation of the change of fluid composition due to asphaltene precipitation.

To solve the compositional phase equilibrium within the reservoir simulator, mass balance and volume balance formulations are equivalent in their results. The volume balance type models are only implicit in pressure; basically the formulation is an IMPESC approach (Cao, 2002). The mass balance formulation can be solved either as fully-implicit or as IMPESC, allowing additional flexibility for adapting to specific problems.

Fully-implicit methods are completely stable when solving the governing equations as all unknowns are solved at the same time. This allows larger time steps, but it also requires larger computer memory. IMPESC formulations have the advantage of being simpler to solve and to program, but being potentially unstable. The computations require small time steps for reaching convergence.

The consideration of asphaltene precipitation and subsequent formation damage, further increases the non-linearity and tightly-coupling of fluid, rock, and pressure when formulating the equations. An IMPESC solution method successfully deals with these interactions and preserves computational efficiency, memory requirements, and simplicity for programming (Liu, 1997). Therefore, a formulation based on mass balance, IMPESC solution, and the Acs et al. procedure will be used for the development of the 3D reservoir simulator.

CHAPTER III
PHASE EQUILIBRIUM MODEL

This chapter outlines the phase behavior model for predicting asphaltene precipitation from live oils. First, we describe the main cubic equations of state currently used in the oil industry for reservoir simulation, followed by the fundamentals of general phase equilibrium and formulation of a three-phase flash VLLE algorithm. Later, we define the steps to perform an stability analysis: a first test is performed using Rachford-Rice equation to determine the formation of liquid and vapor phase, while a second test determines the formation of asphaltene phase from the existing liquid phase. Thermodynamic stability is found when the fugacity of each component is equal in every existing phase, also known as iso-fugacity criteria. The algorithm described in this chapter was implemented and it is validated as shown in Chapter IV.

3.1 Equations of state

An equation of state (EOS) is a functional relationship between state functions describing the equilibrium state of a system. These equations accurately represent the dynamics of phase behavior caused by perturbing thermodynamic properties, including pressure, volume, temperature, and composition.

In the oil industry, it is more common to use semi-empirical cubic EOS to predict fluid behavior of petroleum mixtures. These equations were derived from the theoretical basis of van der Waals (1873), who accounted for non-zero molecular volume at infinite pressure (b) and attraction and repulsion forces between molecules (a). More recent modifications resulted in equations with more reliable quantitative predictions, more commonly used Soave-Redlich-Kwong and Peng-Robinson EOS. These equations have been widely used to calculate fluid properties and model phase behavior in compositional reservoir simulators.

3.1.1 Soave-Redlich-Kwong equation

In 1972, Soave proposed a modification of the equation of state developed by Redlich and Kwong (1949); this equation is known as Soave-Redlich-Kwong (SRK) EOS. Soave suggested replacing the temperature dependent term a for a more general form, resulting in Eq. 3.1 to calculate the pressure of a system, where p is pressure, R is gas constant, T is temperature, V_m is molar volume, and a and b are equation parameters representing repulsion and volume at inifite pressure.

$$p = \frac{RT}{V_m - b} - \frac{a}{V_m(V_m + b)} \tag{3.1}$$

Eq. 3.1 can also be written in terms of compressibility factor Z, as show in Eq. 3.2, where A and B are given by Eq. 3.3 and Eq. 3.4. This expression is more commonly used for solving computational problems.

$$Z^3 - Z^2 + (A - B - B^2)Z - (AB) = 0 \tag{3.2}$$

$$A = \frac{ap}{(RT)^2} \tag{3.3}$$

$$B = \frac{bp}{RT} \tag{3.4}$$

For a pure component, parameters a and b are calculated using Eq. 3.5 and Eq. 3.6, where T_{c_i} is the critical temperature, P_{c_i} is the critical pressure, and α_i depends on the value of the acentric factor ω_i as shown in Eq. 3.7. Subindex i refers to the component index.

$$a = a_i = 0.45724\frac{R^2 T_{c_i}^2}{P_{c_i}^2}\alpha_i \tag{3.5}$$

$$b = b_i = 0.07780\frac{RT_{c_i}}{P_{c_i}} \tag{3.6}$$

$$\alpha_i = \left[1 + \left(0.480 + 1.574\omega_i - 0.176\omega_i^2\right)\left(1 - \sqrt{\frac{T}{T_{c_i}}}\right)\right]^2 \tag{3.7}$$

Another important concept is the corrected pressure for non-ideal fluids, which is defined by the fugacity, f_i, or the fugacity coefficient, φ_i. This property is used in the formulation for phase equilibrium and it's continuously calculated in a compositional reservoir simulator. For a pure component using SRK EOS, it is calculated using the following equation.

$$\ln(\varphi_i) = \ln\left(\frac{f_i}{p}\right) = (Z-1) - \ln(Z-B) - \frac{A}{B}\ln\left(1 + \frac{B}{Z}\right) \tag{3.8}$$

Similar equations are developed for mixtures of i to N_c components. The component parameters (a_i, a_j and b_i) are calculated using Eq. 3.5 and Eq. 3.6 described previously for a pure component. Parameters a and b are calculated using Eq. 3.9 and Eq. 3.10, where z is the mole fraction and κ_{ij} is the binary interaction coefficient between components i and j.

$$a = \sum_{i=1}^{Nc}\sum_{j=1}^{Nc} z_i z_j \left(1 - \kappa_{ij}\right) a_i^{0.5} a_j^{0.5} \tag{3.9}$$

$$b = \sum_{i=1}^{Nc} z_i b_i \tag{3.10}$$

The fugacity of component i ($\widehat{f}_i^{\ell}$) in phase ℓ and the mixture fugacity coefficient ($\widehat{\varphi}_i^{\ell}$), are calculated using Eq. 3.11.

$$\ln\left(\widehat{\varphi}_i^{\ell}\right) = \ln\left(\frac{\widehat{f}_i^{\ell}}{z_i\, p}\right) = \frac{b_i}{b}\left(Z^{\ell}-1\right) - \ln\left(Z^{\ell}-B\right) - \frac{A}{B}\left[\frac{2\sum_{j=1}^{Nc} z_j a_i^{0.5} a_j^{0.5}\left(1-\kappa_{ij}\right)}{\alpha} - \frac{b_i}{b}\right]\ln\left(\frac{B}{Z^{\ell}}\right) \tag{3.11}$$

3.1.2 Peng-Robinson equation

In 1976, Peng and Robinson modified Eq. 3.1 in order to improve the liquid density predictions. The result was Eq. 3.12 to calculate the pressure of a system.

$$p = \frac{RT}{V_m - b} - \frac{a}{V_m(V_m+b)+b(V_m-b)} \tag{3.12}$$

Eq. 3.12 can also be written in terms of Z compressibility factor as shown in Eq. 3.13, where A and B are given by Eq. 3.14 and Eq. 3.15.

$$Z^3 - (1-B)Z^2 + (A - 3B^2 - 2B)Z - (AB - B^2 - B^3) = 0 \tag{3.13}$$

$$A = \frac{ap}{(RT)^2} \tag{3.14}$$

$$B = \frac{bp}{RT} \tag{3.15}$$

For a pure component, parameters a and b are calculated using Eq. 3.16 and Eq. 3.17.

$$a = a_i = 0.45724\frac{R^2 T_{c_i}^2}{P_{c_i}^2}\alpha_i \tag{3.16}$$

$$b = b_i = 0.07780\frac{RT_{c_i}}{P_{c_i}} \tag{3.17}$$

Robinson and Peng (1978) modified the calculation of α_i depending on the value of the acentric factor ω_i. Eq. 3.18 is used for $\omega_i \leq 0.5$ while Eq. 3.19 for $\omega_i > 0.5$.

$$\alpha_i = \left[1 + \left(0.037464 + 1.54226\omega_i - 0.26992\omega_i^2\right)\left(1 - \sqrt{\frac{T}{T_{c_i}}}\right)\right]^2 \tag{3.18}$$

$$\alpha_i = \left[1 + \left(0.037464 + 1.485\omega_i - 0.1644\omega_i^2 + 0.01667\omega_i^3\right)\left(1 - \sqrt{\frac{T}{T_{c_i}}}\right)\right]^2 \tag{3.19}$$

Fugacity for a pure component is therefore calculated using the following equation.

$$\ln(\varphi_i) = \ln\left(\frac{f_i}{p}\right) = (Z-1) - \ln(Z-B) - \frac{A}{2\sqrt{2}B}\ln\left(\frac{Z + 2.414B}{Z - 0.414B}\right) \tag{3.20}$$

On the other hand, for a mixture of N_c components, a and b are calculated with Eq. 3.21 and Eq. 3.22 respectively. Parameters a_i, a_j and b_i are calculated using Eq. 3.16 and Eq. 3.17 respectively.

$$a = \sum_{i=1}^{Nc}\sum_{j}^{Nc} z_i z_j \left(1 - \kappa_{ij}\right) a_i^{0.5} a_j^{0.5} \tag{3.21}$$

$$b = \sum_{i=1}^{Nc} z_i b_i \tag{3.22}$$

The fugacity of the fluid mixture is calculated using Eq. 3.23.

$$\begin{aligned}\ln(\widehat{\varphi}_i) = \ln\left(\frac{\widehat{f}_i^{\,\ell}}{z_i\, p}\right) &= \frac{b_i}{b}\left(Z^\ell - 1\right) - \ln\left(Z^\ell - B\right) \\ &\quad - \frac{A}{2\sqrt{2}B}\left[\frac{2\sum_{j=1}^{Nc} z_j a_i^{0.5} a_j^{0.5}\left(1 - \kappa_{ij}\right)}{\alpha} - \frac{b_i}{b}\right]\ln\left(\frac{Z + 2.414B}{Z - 0.414B}\right)\end{aligned} \tag{3.23}$$

For this research, Peng-Robinson EOS was chosen and used for deriving the asphaltene precipitation model and perform subsequent testing and validation. However, the same procedure can be implemented using any cubic equation of state.

3.2 Phase equilibrium

In a multiphase system, the number of phases coexisting in equilibrium is determined by a stability analysis. The system is said to be in equilibrium when the total Gibbs energy (G_t) is minimum, therefore, a fluid mixture will continuously split into additional phases until Gibbs energy can not be reduced any further. **Fig. 3.1** shows the stability analysis that determines the number of phases by comparing the total Gibbs energy in one, two, and three phases. For this example, if G^1 is lower than G^2, then only one phase exists. However, if G^2 is lower than G^1, then the fluid would be more stable by creating a second phase. Similarly, the fluid exists in at least three-phases when G^3 is lower than G^2 and G^1.

(a) 1-phase $G_t = G^1$
$G^1 \leq G^2, G^3$

(b) 2-phases $G_t = G^2$
$G^2 \leq G^1, G^3$

(c) 3-phases $G_t = G^3$
$G^3 \leq G^1, G^2$

Fig. 3.1—Stability analysis to determine the number of phases existing in equilibrium considering liquid, gas, and solid phase. The mixture exists at conditions where the total Gibbs energy is minimum.

Gibbs free energy is a function of pressure, temperature, and the number of moles of each component (n_i), as shown in Eq. 3.24. Starting from this concept, we can define the condition for stability used in a flash calculation.

$$G = f(p, T, n_1, ..., N_c) \tag{3.24}$$

Differentiating the previous equation results in Eq. 3.25. For a system with constant pressure and constant temperature, this can be reduced to Eq. 3.26.

$$dG = \left(\frac{\partial G}{\partial p}\right)_{T,n} dp + \left(\frac{\partial G}{\partial T}\right)_{p,n} dT + \sum_{i=1}^{N_c} \left(\frac{\partial G}{\partial n_i}\right)_{p,T,n_j} dn_i \tag{3.25}$$

$$dG = \sum_{i=1}^{N_c} \left(\frac{\partial G}{\partial n_i}\right)_{p,T,n_j} dn_i \tag{3.26}$$

The chemical potential μ of component i as a function of Gibbs energy is defined as:

$$\mu_i = \left(\frac{\partial G}{\partial n_i}\right)_{p,T,n_j} dn_i \tag{3.27}$$

Combining Eq. 3.26 and Eq. 3.27, we define the derivative of Gibbs free energy as a function of chemical potential, as shown in Eq. 3.28.

$$dG = \sum_{i=1}^{N_c} \mu_i dn_i \tag{3.28}$$

For a three-phase system, we can apply Eq. 3.28 to each phase. Superindices v, l, and s represents vapor, liquid, and solid phase respectively.

$$dG^v = \sum_{i=1}^{N_c} \mu_i^v dn_i^v \tag{3.29}$$

$$dG^l = \sum_{i=1}^{N_c} \mu_i^l dn_i^l \tag{3.30}$$

$$dG^s = \sum_{i=1}^{N_c} \mu_i^s dn_i^s \tag{3.31}$$

The sum of Gibbs free energies of all phases in a multi-phase system must add to zero. Combining Eq. 3.29 to Eq. 3.31, we have:

$$\begin{aligned} (dG)_{p,T} &= (dG^v)_{p,T} + (dG^l)_{p,T} + (dG^s)_{p,T} = 0 \\ &= \sum_{i=1}^{N_c} \mu_i^v dn_i^v + \sum_{i=1}^{N_c} \mu_i^l dn_i^l + \sum_{i=1}^{N_c} \mu_i^s dn_i^s = 0 \end{aligned} \tag{3.32}$$

For a closed system, mass is preserved at all times (Eq. 3.33). After algebraic manipulation of Eq. 3.32 and Eq. 3.33, we obtain Eq. 3.34. This equation is satisfied when the chemical potential of any component i is equal for all its phases. Therefore, Eq. 3.35 is the equilibrium condition for a three-phase system.

$$dn_i{}^v + dn_i{}^l + dn_i{}^s = 0 \tag{3.33}$$

$$\sum_{i=1}^{N_c} (\mu_i^l - \mu_i^v) dn_i^l + \sum_{i=1}^{N_c} (\mu_i^s - \mu_i^v) dn_i^s = 0 \tag{3.34}$$

$$\mu_i^l = \mu_i^v = \mu_i^s \tag{3.35}$$

The relationship between the chemical potential of a component can also be expressed in terms of fugacity. These two concepts relate to each other as:

$$d\mu_i = RTd \ln f_i \tag{3.36}$$

Integrating Eq. 3.36, we have:

$$\mu_i = \mu_i^0 + RT \ln f_i \tag{3.37}$$

Combining Eq. 3.35 and Eq. 3.37, we can express the final equilibrium condition as a function of fugacity for a three-phase system: liquid, vapor, and solid. This is the concept that we used in the development of the flash for predicting asphaltene precipitation.

$$f_i^l = f_i^v = f_i^s \tag{3.38}$$

3.3 Vapor/liquid/liquid-dense model

For modeling asphaltene precipitation, we used conventional liquid/liquid split described with Peng-Robinson EOS. The model is based on the following assumptions:

1. A maximum of three phases can be formed: vapor, liquid, and solid.

2. Solid asphaltene is modeled with a cubic equation of the state as a liquid-dense phase.

3. Solid phase is considered pure asphaltene (one pseudo-component). This assumption is acceptable given the definition, and laboratory quantification, that describes asphaltene as petroleum fractions insoluble in paraffin solvents, therefore all precipitated under these conditions should be considered as a unique asphaltene phase. This assumption simplify the computation requirements, as the solubility of other components in the solid phase is neglected. Fugacity for a pure component is calculated using the equations described previously in this chapter.

4. Asphaltene can only exists in liquid and solid phase. Asphaltene content in the vapor phase is neglected due its low volatility. This assumption will not consider asphaltene precipitation from the vapor phase, therefore, we only performed an asphaltene stability test when a liquid phase exists.

A system is in equilibrium when the iso-fugacity criteria is satisfied. This occurs when the fugacities of all components (or pseudo-component) are equal in every phase, as shown in Eq. 3.39.

$$\widehat{f}_i^{\,l} = \widehat{f}_i^{\,v} = f_i^{s} \tag{3.39}$$

The material balance of the system is defined by the phase mole fraction f summing to unity (Eq. 3.40), and the component mole fraction z following Eq. 3.41, where x_i is the liquid mole fraction and y_i is the vapor mole fraction of component i.

$$f_v + f_l + f_s = 1 \tag{3.40}$$

$$z_i = \begin{cases} f_v y_i + f_l x_i, & \text{For } i \neq \text{asphaltene} \\ \\ f_l x_i + f_s, & \text{For } i = \text{asphaltene} \end{cases} \tag{3.41}$$

The general procedure to solve the equilibrium flash with asphaltene precipitation is shown in **Fig. 3.2**. With pressure, temperature, and overall composition, we perform a conventional vapor/liquid equilibrium (VLE), assuming only these two-phases could exist. From this calculation we have three possible scenarios: 100% liquid, two-phase liquid/vapor, and 100% vapor. If the fluid is found to be all in vapor state, then we conclude that asphaltene would not precipitate from the mixture (based on assumption 4).

On the other hand, if VLE results in the formation of a liquid phase (single or two-phase), then we perform a second stability test to check whether the mixture is unstable and will trigger the formation of an additional liquid-dense phase (asphaltene). If the fluid is found to be stable, then we keep the result from the VLE. If the fluid is not stable, we iterate on the liquid asphaltene fraction until satisfying Eq. 3.39, Eq. 3.40, Eq. 3.41. This procedure

for each stability system is explained in following sections.

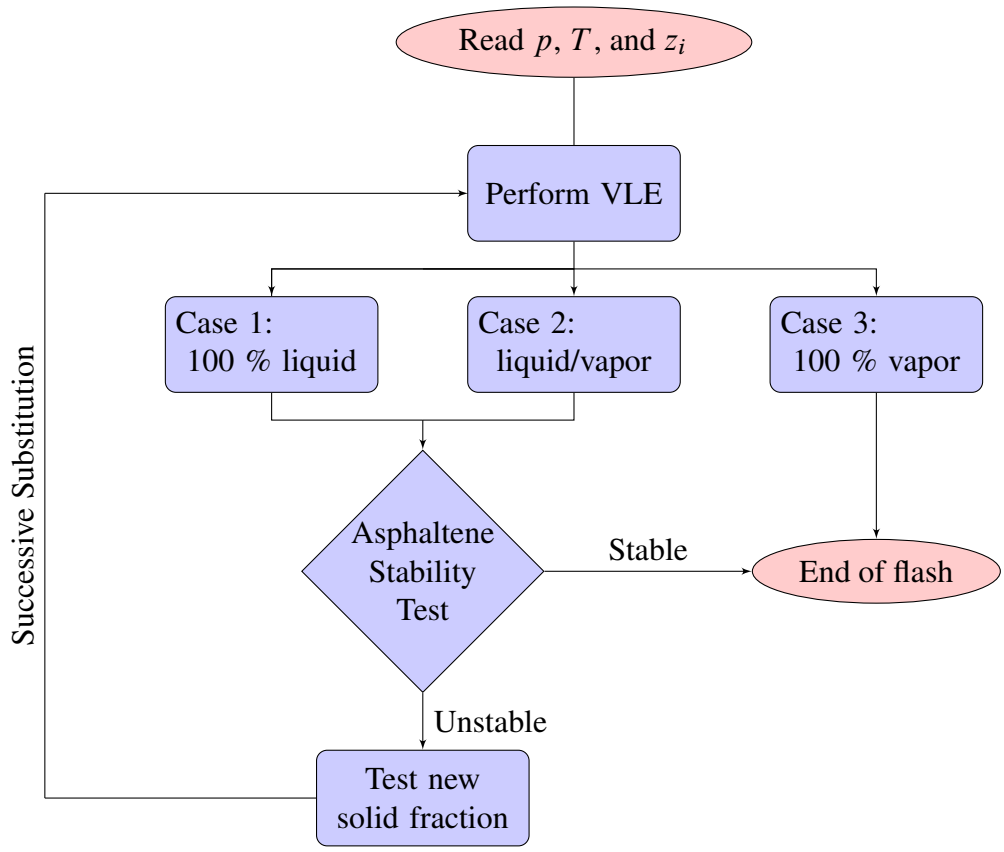

Fig. 3.2—General flowchart for asphaltene precipitation using a three-phase flash solved using successive substitution. First, a conventional VLE will determine if there is a liquid phase. A second stability analysis is performed in the liquid to determine if a new asphaltene fraction will be formed.

3.3.1 Vapor/liquid system

The first step in determining asphaltene precipitation is to perform a conventional two-phase vapor/liquid flash equilibrium. It is calculated given pressure, temperature, and overall composition. This provides number of phases, moles in each phase, and molar fraction for the phases. The flash is defined by the following relations:

1. General phase equilibrium represented by Eq. 3.42, where the fugacity of each component is equal in vapor and liquid phase.

$$\widehat{f}_i^{\,l} = \widehat{f}_i^{\,v} \tag{3.42}$$

2. Material balance equation for each component represented by Eq. 3.43.

$$z_i = f_v y_i + (1 - f_v) x_i \tag{3.43}$$

3. The components' mole fractions for each phase sum to unity as shown in equation Eq. 3.44.

$$\sum_{i=1}^{Nc} (y_i - x_i) = 0 \tag{3.44}$$

Fugacities (Eq. 3.42) are a function of pressure and fugacity coefficient, defined in Eq. 3.45 and Eq. 3.46.

$$\widehat{f}_i^{\,l} = x_i \widehat{\varphi}_i^{\,l} p \tag{3.45}$$

$$\widehat{f}_i^{\,v} = y_i \widehat{\varphi}_i^{\,v} p \tag{3.46}$$

We define K-values for component i as follow:

$$K_i = \frac{y_i}{x_i} \tag{3.47}$$

Combining Eq. 3.45- 3.47, we establish the equilibrium relationship in terms of K-values.

$$K_i = \frac{y_i}{x_i} = \frac{\widehat{\varphi}_i^{\,l}}{\widehat{\varphi}_i^{\,v}} \tag{3.48}$$

Substituting Eq. 3.48 into our second equilibrium condition (Eq. 3.43), we can establish the material balance constraints (Eq. 3.49 and Eq. 3.50).

$$x_i = \frac{z_i}{1 - f_v + f_v K_i} \tag{3.49}$$

$$y_i = \frac{K_i z_i}{1 - f_v + f_v K_i} \tag{3.50}$$

Combining Eq. 3.49 and Eq. 3.50 yields the standard method for calculating a two-phase flash, originally proposed by Rachford and Rice (1952).

$$\sum_{i=1}^{Nc} (y_i - x_i) = \sum_{i=1}^{Nc} \frac{z_i (K_i - 1)}{1 - f_v + f_v K_i} = 0 \tag{3.51}$$

The procedure for solving a liquid/vapor equilibrium was summarized by Firoozabadi (1999) in the following steps:

1. Get initial estimates for K-values using the approximation proposed by Wilson (1969).

$$\ln K_i = \ln\left(\frac{P_{c_i}}{p}\right) + 5.373\,(1 + \omega_i)\left(1 - \frac{T_{c_i}}{T}\right) \tag{3.52}$$

2. Solve Eq. 3.51 using Newton's method to find f_v.

3. Calculate mole fraction of each component using Eq. 3.49 and Eq. 3.50.

4. Calculate the fugacity coefficient of each component using Eq. 3.23.

5. Update K_i given by Eq. 3.53.

$$K_i^{n+1} = K_i^n \left(\frac{\widehat{\varphi}_i^v}{\widehat{\varphi}_i^l}\right) \tag{3.53}$$

6. Test whether convergence is achieved using $\epsilon \leq 1 \times 10^{-14}$, where ϵ is given by Eq. 3.54.

$$\epsilon = \sum_{i=1}^{Nc} \frac{z_i \left(K_i - 1\right)}{1 - f_v + f_v K_i} \tag{3.54}$$

7. If convergence is not satisfied, then update K-values with Eq. 3.55 and repeat Steps 2 through 7.

$$K_i^{n+1} = K_i^n \left(\frac{\widehat{f}_i^{\,l}}{\widehat{f}_i^{\,v}} \right) \tag{3.55}$$

3.3.2 Liquid/liquid system

To test whether asphaltene precipitates from the existing liquid phase, a second stability test is performed. The fugacity of asphaltene as a pure component is compared with the liquid fugacity of asphaltene in the mixture. As explained in Section 3.2, asphaltene precipitates if the fugacity of asphaltene in the liquid mixture is greater than the fugacity of the asphaltene in pure solid state. This relationship is shown in Eq. 3.56, indicating that the fluid would be more stable with the formation of an additional phase (asphaltene).

$$\widehat{f}_{asph}^{\,l} > f_{asph}^{s} \tag{3.56}$$

The amount of asphaltene precipitated is calculated by iterating the number of moles of asphaltene removed from the liquid mixture. Once the fugacity of asphaltene in the liquid mixture equals the fugacity as a pure component, the fluid is found in equilibrium. The number of asphaltene moles calculated in the liquid mixture represents the maximum asphaltene that can be in liquid state for a thermodynamically stable system. The excessed moles precipitate into a pure liquid-dense phase. This process is illustrated in **Fig. 3.3**.

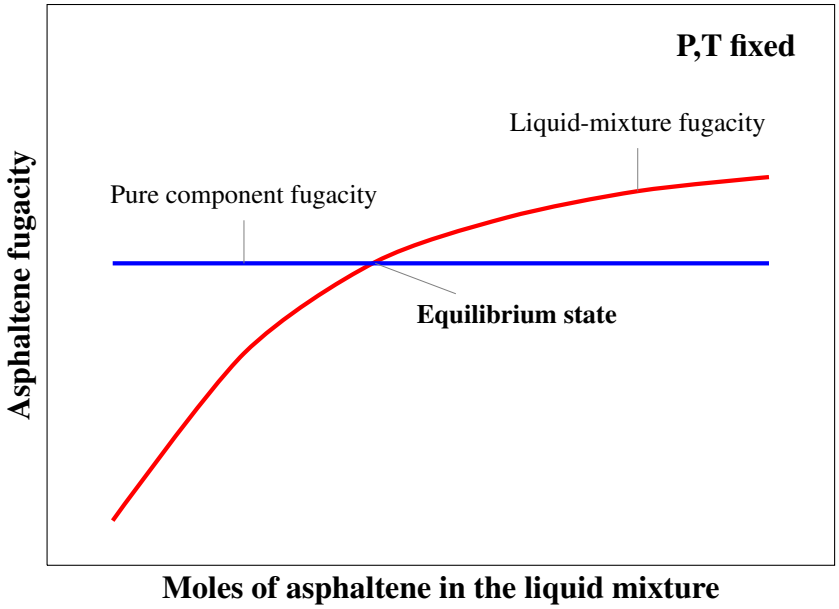

Fig. 3.3—Stability of asphaltene in a liquid/liquid split. The equilibrium state is found when the fugacity of asphaltene as a pure component equals the fugacity of asphaltene in the liquid mixture.

The procedure to calculate the three-phase equilibrium is summarized in the following steps:

1. Complete a two-phase flash considering vapor and liquid as shown in Section 3.3.1. Compute fugacity of asphaltene component within the liquid mixture using Eq. 3.23.

2. Calculate fugacity of asphaltene as a pure phase using Eq. 3.20.

3. Perform a stability analysis test to determine if asphaltene will precipitate based on the criteria established in Eq. 3.56.

4. If asphaltene precipitates, calculate a new composition of the asphaltene component dissolved in the mixed liquid phase using the following equation.

$$z_{asph}^{n+1} = (0.5) z_{asph}^{n} \tag{3.57}$$

5. Re-normalize composition and repeat a two-phase flash as shown in Section 3.3.1. Compute the liquid fugacity of the asphaltene component.

6. Test if convergence criterion is achieved using $\epsilon \leq 1 \times 10^{-14}$, where ϵ is given by Eq. 3.58.

$$\epsilon = \widehat{f}^{l}_{asph} - f^{s}_{asph} \tag{3.58}$$

7. If the criterion is not met, then update z_{asph} using Eq. 3.59 and repeat steps 5 to 7 until convergence criterion is satisfied.

$$z^{n+1}_{asph} = z^{n}_{asph} \left(\frac{f^{s}_{asph}}{\widehat{f}^{l}_{asph}} \right) \tag{3.59}$$

CHAPTER IV
PHASE BEHAVIOR PREDICTION

This chapter is divided into four main sections, the first part includes a validation of the model by comparing our mathematical predictions versus laboratory experiments obtained by Burke et al. (1990). The reproducibility tests were performed for the following cases: constant temperature and constant composition at different pressures, and solvent injection at different concentration. In addition, an analysis of asphaltene precipitation at different temperatures was performed and compared to the general behavior observed by Hirschberg et al. (1984) and Leontaritis (1996).

The second part presents a sensitivity analysis, where the main asphaltene characterization parameters (P_c, T_c, ω, and κ_{ij}) were varied to understand their effect on the final asphaltene precipitation. And the fourth section evaluates the algorithm efficiency and additional computational cost by comparing the CPU time required for a three-phase flash (vapor/liquid/liquid) and for a two-phase (vapor/liquid) calculation. A CPU comparison between the dense-liquid model and the solid model is performed to account the additional cost to implement a more consistent thermodynamic model.

4.1 Reproducibility of experimental data

To evaluate the validity of the vapor/liquid/liquid-dense model and the reproducibility of experimental data, we compared our model predictions with the laboratory results obtained and published by Burke et al. in 1990. The authors performed experiments using live oil fluids with API gravities ranging from 19° to 40° mixed with different solvents. To measure the amount of asphaltene precipitated, Burke et al. constructed a high-pressure piston cell with removable end caps and steel balls to mix oil and solvent.

Their experimental procedure, consisted of injecting a reservoir fluid into a sealed cell using pressures and temperatures representing downhole reservoir conditions. The solvent mixture was subsequently added at the desired proportion. The cell would remain undisturbed during 24 hours to allow the asphaltene to precipitate and adhere to the bottom of the cell. The asphaltene recovered was rinsed with heptane to remove resins or waxes. The amount of asphaltene precipitated was reported in weight percentage of live oil.

Two types of experiments were compared based on Burke et al.'s experiments: asphaltene precipitation at different pressures with fixed composition and temperature, and asphaltene precipitation with solvent injection at fixed pressure and temperature. **Table 4.1** describes the composition of two oils and one solvent used in this study to validate the asphaltene prediction model. Oil 1 and 2 are found in liquid state, while solvent is in gas state at standard conditions but as supercritical at working conditions (temperature of 180 °F).

4.1.1 Precipitation with pressure

The pressure test is designed to observe and understand the effect of pressure and temperature in the overall asphaltene precipitation. These experiments contained only live oil in the cell, recording the amount of asphaltene precipitated at different pressure values. Burke et al. measured asphaltene precipitation of Oil 1 at pressures ranging from 1,014.7 psia to 4,014.7 psia. The results of these experiments are shown in **Table 4.2**.

The asphaltene fraction of Oil 1 was characterized by splitting the C_{7+} pseudo-component into two new fractions, precipitating (asphaltene) and nonprecipitating. To match the experimental data, we regressed on molecular weight, precipitating/nonprecipitating mole ratio, binary interaction coefficients between asphaltene and components ligher than C_1, and critical properties of the nonprecipitating and the asphaltene fraction.

TABLE 4.1—MOLAR COMPOSITION (%) OF OILS AND SOLVENT USED TO VALIDATE THE ASPHALTENE PRECIPITATION MODEL (BURKE, 1990)

	Fluid z_i (%)		
Component	**Oil 1**	**Oil 2**	**Solvent**
N_2	0.57	0.51	3.17
CO_2	2.46	1.42	17.76
C_1	36.37	6.04	30.33
C_2	3.47	7.00	26.92
C_3	4.05	6.86	13.09
iC_4	0.59	0.83	1.26
nC_4	1.34	3.35	4.66
iC_5	0.74	0.70	0.77
nC_5	0.83	3.46	1.26
C_6	1.62	3.16	0.78
C_{7+}	47.96	66.68	0.00
C_{7+} Molecular weight	329	281	
C_{7+} Specific gravity	0.9594	0.902	
API gravity	19	24	
Reservoir temperature, °F	212	218	
Saturation pressure, psia	2,950	600	

TABLE 4.2—AMOUNT OF ASPHALTENE PRECIPITATED FROM OIL 1 AT PRESSURES RANGING FROM 1,014.7 PSIA TO 4,014.7 PSIA (BURKE, 1990)

Test pressure (psia)	**Precipitates from live oils (wt%)**
1,014.7	0.403
2,014.7	1.037
3,034.7	0.742
4,014.7	0.402

Molecular weight of each fraction was estimated using the average molecular weight of C_{7+}, measured in the laboratory, and the precipitating/nonprecipitating mole ratio. This relation is shown in Eq. 4.1.

$$Mw_{C_{7+}} = Mw_{asph} \times z_{i_{asph}} + Mw_{C_{7+}^{nonprec}} \times z_{C_{7+}^{nonprec}} \tag{4.1}$$

Fig. 4.1 shows the asphaltene precipitation of the vapor/liquid/liquid-dense model (continuous solid line) compared to the experimental data (cross markers). The fluid properties for this match are shown in **Table 4.3**, with a bubble point of 2,200 psia and the maximum precipitation of 1.094 wt% observed near that point. The model was not able to reproduce the reported bubble point pressure of 2,950 psia while matching the precipitation percentage at every pressure.

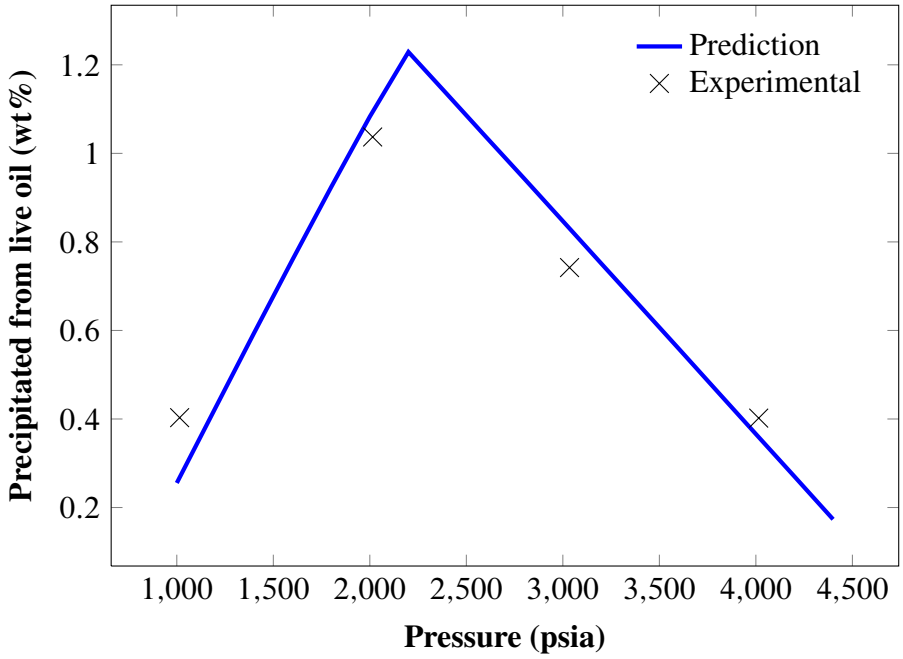

Fig. 4.1—Match of Burke et al.'s experiment for Oil 1: asphaltene precipitation with pressure. The prediction matches all experimental data points resulting in a bubble point pressure of 2,220 psia and a maximum precipitation of 1.094 wt% near that point.

This experiment was previously simulated numerically by Nghiem (1999) using the vapor/liquid/solid model described in Chapter II. In his studies, Nghiem reported inconsistencies between Burke et al.'s experimental data and the predictions from his model.

TABLE 4.3—FLUID PROPERTIES USED FOR OIL 1 MATCHING BURKE ET AL.'S EXPERIMENTS

Component	**Mw**	**Pc (psia)**	**Tc (F)**	ω	z_i **(%)**
N_2	28.00	492.5	-232.8	0.040	0.57
CO_2	44.01	1,070.2	87.6	0.225	2.46
C_1	16.04	667.4	-116.9	0.008	36.37
C_2	30.00	708.5	89.7	0.098	3.47
C_3	44.10	615.9	205.6	0.152	4.05
iC_4	58.10	529.2	274.6	0.176	0.59
nC_4	58.10	551.3	305.4	0.193	1.34
iC_5	72.20	491.0	368.7	0.227	0.74
nC_5	72.20	489.5	385.3	0.251	0.83
C_6	86.00	477.2	453.5	0.275	1.62
$C_{7+}^{nonprec}$	310.00	180.6	955.0	1.019	47.16
$Asphaltene$	780.00	179.0	2,056.0	1.404	0.80

Binary Interaction Coefficient

$Asphaltene-$ light components (C_1 to C_5) 0.047

He concluded, as previously suggested in the literature, that the maximum precipitation should occur near the bubble point pressure, which is the lowest pressure at which the gas solubility is at a maximum.

Burke et al.'s experimental data shows the maximum precipitation around 2,000 psia rather than near the measured bubble point pressure of 2,950 psia. Due to these theoretical inconsistencies, Nghiem (1999) proposed matching the observed data neglecting the results obatined at 1,014.7 psia and 2,014.7 psia. This way, the maximum asphaltene precipitation would occur around 3,000 psia, near the bubble point pressure.

This conclusion is based on the fact that measuring the amount of asphaltene precipitated is often complex and it may result in experimental errors. On the other hand, the measurement of bubble point pressure is a routine experiment that leaves little error. For this case, the precipitation behavior proposed by Nghiem seems to be more adequate for a fluid at

constant composition and reported bubble point pressure of 2,950 psia. The results obtained by Nghiem were used as a reference, where only the experimental points at 3,014.7 psia and 4,014.7 psia were used for the match.

The match of Oil 1 based on Nghiem's interpretation is shown in **Fig. 4.2**, while **Table 4.4** display the fluid properties. The calculated bubble point pressure is 2,953 psia, matching the the last two points observed by Burke et al.

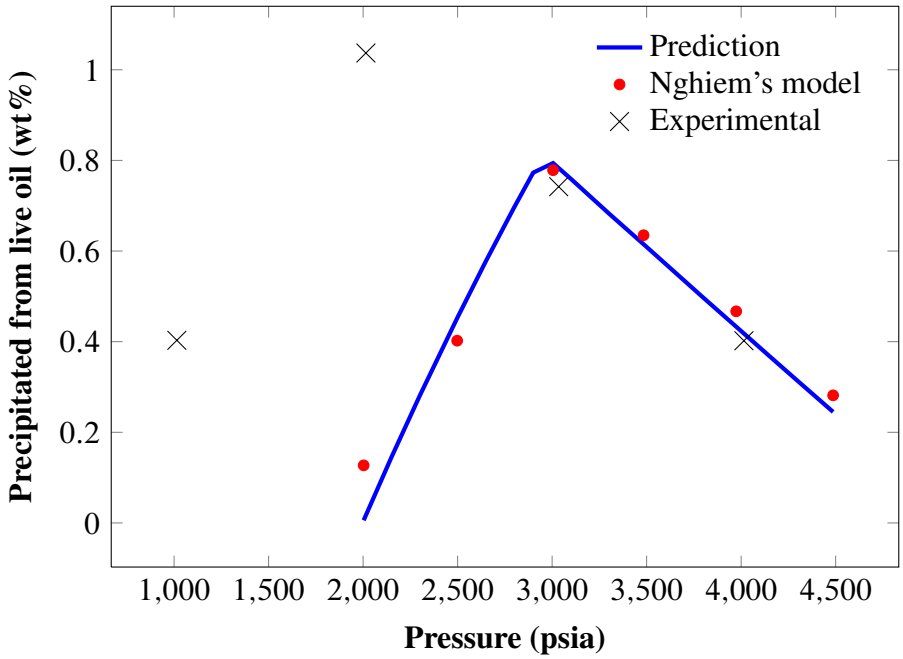

Fig. 4.2—Match of Burke et al.'s experiment Oil 1: asphaltene precipitation with pressure based on Nghiem's interpretation. The prediction results in a bubble point pressure of 2,953 psia, which matches the laboratory measurement and Nghiem's model.

Fig. 4.3 shows the complete asphaltene precipitation envelope using the fluid description from Table 4.4. It includes the pressure at which asphaltene starts to precipitate (lower AOP), the maximum precipitation at saturation point, and the asphaltene redissolution effect (upper AOP). The figure demonstrates the ability of the model to reproduce and predict the upper and the lower asphaltene onset pressure (AOP). This feature is very important

as it shows the ability to predict the interactions between components and its effect on asphaltene solubility when the system undergoes complex changes of composition.

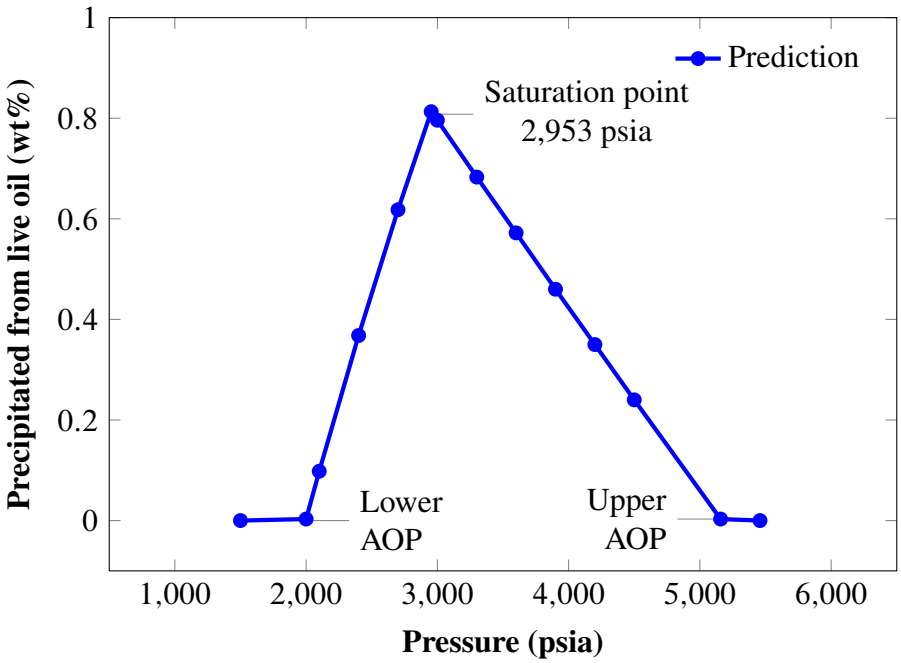

Fig. 4.3—Full asphaltene precipitation curve of Oil 1 (Table 4) at 212 °F showing the ability of the model to reproduce the upper and lower asphaltene onset pressure.

4.1.2 Precipitation with solvent injection

Asphaltene precipitation from Oil 2 was measured after mixing with Solvent at different concentrations, varying its percentage from 0 to 90%. **Table 4.5** shows the overall composition for each mixture. The test pressures and experimental results from Burke are shown in **Table 4.6**.

Fluid characterization for Oil 2 was performed using the same approach previously outlined previously for Oil 1. C_{7+} pseudo-component was split into precipitating and non-precipitating fractions, regressing on the fluid properties to match observed precipitation

data and bubble point pressure (600 psia). The final prediction is shown in **Fig. 4.4**, matching all data points except at solvent concentration of 78%. The properties of the matched fluid are shown in **Table 4.7**.

TABLE 4.4—FLUID PROPERTIES USED FOR OIL 1 BASED ON NHGHIEM'S MATCHING

Component	**Mw**	**Pc (psia)**	**Tc (F)**	ω	z_i **(%)**
N_2	28.00	492.5	-232.8	0.0400	0.570
CO_2	44.01	1,070.2	87.6	0.2250	2.460
C_1	16.04	667.4	-116.9	0.0080	36.370
C_2	30.00	708.5	89.7	0.0980	3.470
C_3	44.10	615.9	205.6	0.1520	4.050
iC_4	58.10	529.2	274.6	0.1760	0.590
nC_4	58.10	551.3	305.4	0.1930	1.340
iC_5	72.20	491.0	368.7	0.2270	0.740
nC_5	72.20	489.5	385.3	0.2510	0.830
C_6	86.00	477.2	453.5	0.2750	1.620
$C_{7+}^{nonprec}$	320.0	180.8	1,089.0	1.022	47.145
$Asphaltene$	800.00	178.3	2,105.0	1.441	0.815

Binary Interaction Coefficient

$Asphaltene-$ light components (C_1 to C_5)	0.135
$C_{7+}^{nonprec} - C_1$	0.053

Up to 70% solvent, the higher the solvent concentration, the higher the amount of asphaltene precipitated. This occurs due to higher asphaltene solubility in heavier mixtures, therefore, asphaltene precipitation is triggered by adding a lighter solvent mixture.

On the other hand, at solvent concentrations greater than 85%, asphaltene precipitation decreases by adding solvent. Burke et al. claimed that the addition of a solvent does not always guarantee additional precipitation and attributed this behavior to changes in fluid properties when the system undergoes retrograde condensation.

Our model was able to simulate the increment in asphaltene precipitation after adding solvent, and the decrease in precipitation at high solvent concentration as it was observed in the experimental data excep for the point at 78 %.

TABLE 4.5—FLUID COMPOSITION AT DIFFERENT PERCENTAGES OF SOLVENT CONCENTRATION

	(moles of solvent/moles of oil)%						
Component	**0**	**20**	**50**	**70**	**78**	**80**	**90**
N_2	0.51	1.04	1.84	2.37	2.58	2.64	2.90
CO_2	1.42	4.69	9.59	12.86	14.17	14.49	16.13
C_1	6.04	10.90	18.19	23.04	24.99	25.47	27.90
C_2	7.00	10.98	16.96	20.94	22.54	22.94	24.93
C_3	6.86	8.11	9.98	11.22	11.72	11.84	12.47
iC_4	0.83	0.92	1.05	1.13	1.17	1.17	1.22
nC_4	3.35	3.61	4.01	4.27	4.37	4.40	4.53
iC_5	0.70	0.71	0.74	0.75	0.75	0.76	0.76
nC_5	3.46	3.02	2.36	1.92	1.74	1.70	1.48
C_6	3.16	2.68	1.97	1.49	1.30	1.26	1.02
$C_{7+}^{nonprec}$	65.77	52.62	32.89	19.73	14.47	13.15	6.58
$Asphaltene$	0.90	0.72	0.45	0.27	0.20	0.18	0.09

TABLE 4.6—RESULTS OF ASPHALTENE PRECIPITATION WITH SOLVENT INJECTION (BURKE, 1990)

Test pressure (psia)	**% Moles injected into the total mix**	**Precipitates from live oils (wt%)**
3,014.7	0	0.14
3,014.7	20	0.27
3,014.7	50	1.46
4,214.7	70	1.65
5,014.7	78	3.21
5,014.7	85	1.29
5,014.7	90	1.10

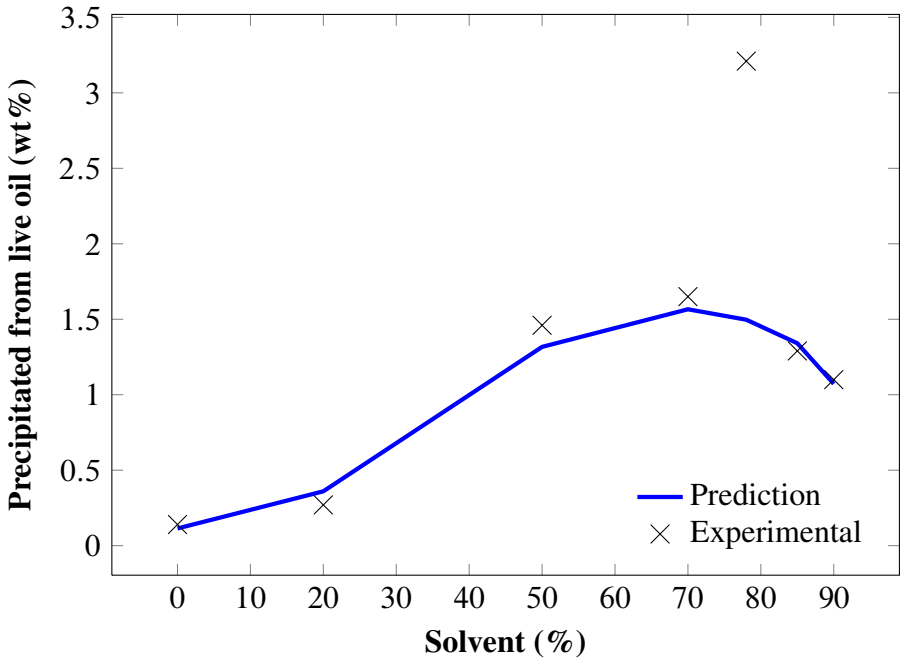

Fig. 4.4—Match of Burke et al.'s experimental data for asphaltene precipitation of Oil 2 using different solvent concentration (from 0% to 90%.) The model predicts increment in precipitation when adding solvent up to 70% due, and decrease in precipitation for concentrations greater than 85%.

4.1.3 Precipitation with temperature

To evaluate the effect of temperature on asphaltene precipitation, we used Oil 1 (Table 4.4). Although there are not laboratory experiments to validate the quantitative prediction of the model, we observed its general behavior to confirm that follows the expected physical tendency.

Fig. 4.5 shows the weight percentage of asphaltene at 2,500 psia and temperatures varying from 60°F to 228°F. The results show that asphaltene precipitation decreases as temperature increases. The increment of asphaltene solubility when temperature is incremented has been previously documented by Hirschberg et al. (1984) and Leontaritis (1996).

TABLE 4.7—FLUID PROPERTIES USED FOR OIL 2 MATCHING BURKE'S EXPERIMENTS

Component	Mw	Pc (psia)	Tc (F)	ω
N_2	28.00	492.5	-232.8	0.040
CO_2	44.01	1,070.2	87.6	0.225
C_1	16.04	667.4	-116.9	0.008
C_2	30.00	708.5	89.7	0.098
C_3	44.10	615.9	205.6	0.152
iC_4	58.10	529.2	274.6	0.176
nC_4	58.10	551.3	305.4	0.193
iC_5	72.20	491.0	368.7	0.227
nC_5	72.20	489.5	385.3	0.251
C_6	86.00	477.2	453.5	0.275
$C_{7+}^{nonprec}$	276.00	208.9	896.7	0.780
$Asphaltene$	700.00	167.2	2,603.0	1.250

Binary Interaction Coefficient

$Asphaltene-$ light components (C_1 to C_5)	0.020
$C_{7+}^{nonprec} - C_1$	0.199
$C_{7+}^{nonprec} - C_2$	0.025

4.2 Sensitivity analysis

Several sensitivity studies were performed on the characterization parameters to understand asphaltene precipitation. This included: critical pressure, critical temperature, acentric factor, and binary interaction coefficients of asphaltene with light components (C_1 to C_5). Oil 1 (Table 4.4) was used for the analyses, where the asphaltene precipitation weight percentage was recorded in every case for pressures ranging between 1,000 psia and 5,000 psia.

4.2.1 Critical pressure

The effect of critical pressure of the asphaltene fraction was evaluated using 177 psia, 178 psia, and 179 psia. The full properties of asphaltene fraction are shown in **Table 4.8**.

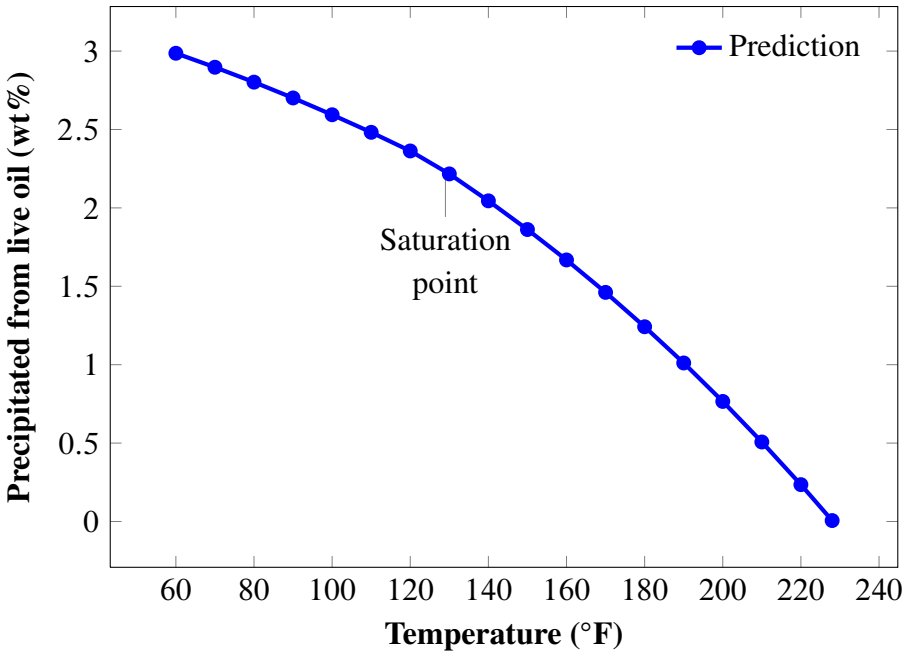

Fig. 4.5—Prediction of asphaltene precipitation at different temperatures with fixed composition (Oil 1) and fixed pressure (2,500 psia). The result shows that precipitation is triggered by decreasing the system temperature.

Fig. 4.6 shows how increasing critical pressure results in a decreased in bubble point pressure and an incremented asphaltene precipitation weight volume. In addition, it extends the ranges of pressures at which asphaltene precipitates, lowering the lower onset pressure, and incrementing the upper onset pressure.

TABLE 4.8—ASPHALTENE PROPERTIES USED FOR CRITICAL PRESSURE SENSITIVITY ANALYSIS USING OIL 1 WHERE X REPRESENTS THE PARAMETER EVALUATED

Component	**Mw**	**Pc (psia)**	**Tc (F)**	ω
$Asphaltene$	800	**X**	2,105	1.441
Binary Interaction Coefficient				
$Asphaltene-$ light components (C_1 to C_5)	0.135			

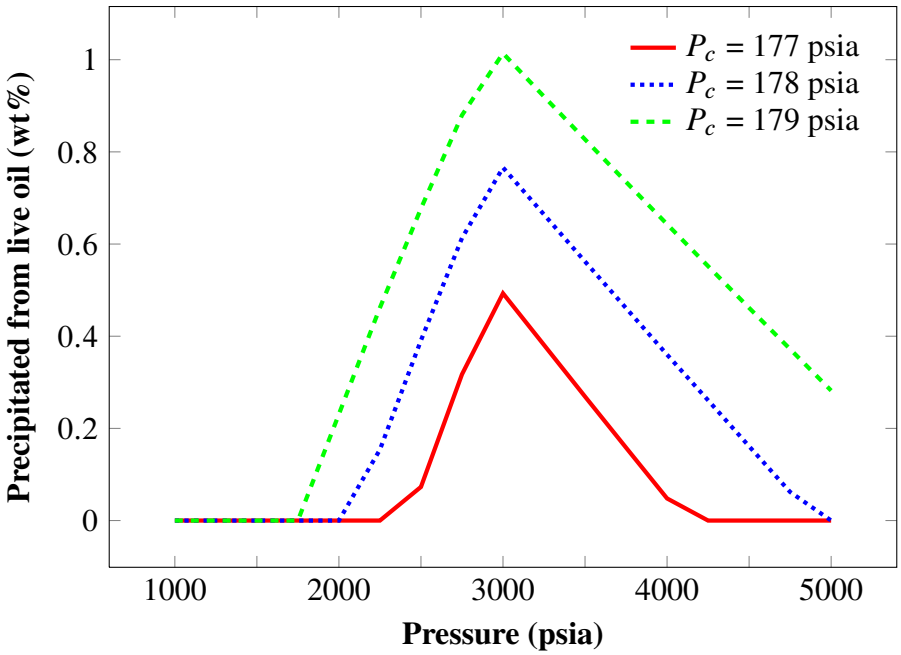

Fig. 4.6—Sensitivity analysis for P_c of the asphaltene pseudo-component using 177 psia, 178 psia, and 179 psia. As the critical pressure increases, asphaltene precipitation increases and bubble point pressure decreases.

4.2.2 Critical temperature

Three different values for critical temperature were used to asses its effect on asphaltene precipitation: 2,090 °F, 2,100 °F, and 2,110 °F. The properties of the asphaltene fraction used during this analysis are shown in **Table 4.9**.

The results from **Fig. 4.7** show an increment in asphaltene precipitation as the the critical temperature increases. Similar to the effect of the critical pressure, increasing the critical temperature also increments the range of pressures at which asphaltene precipitates and reduces the mixture bubble point pressure.

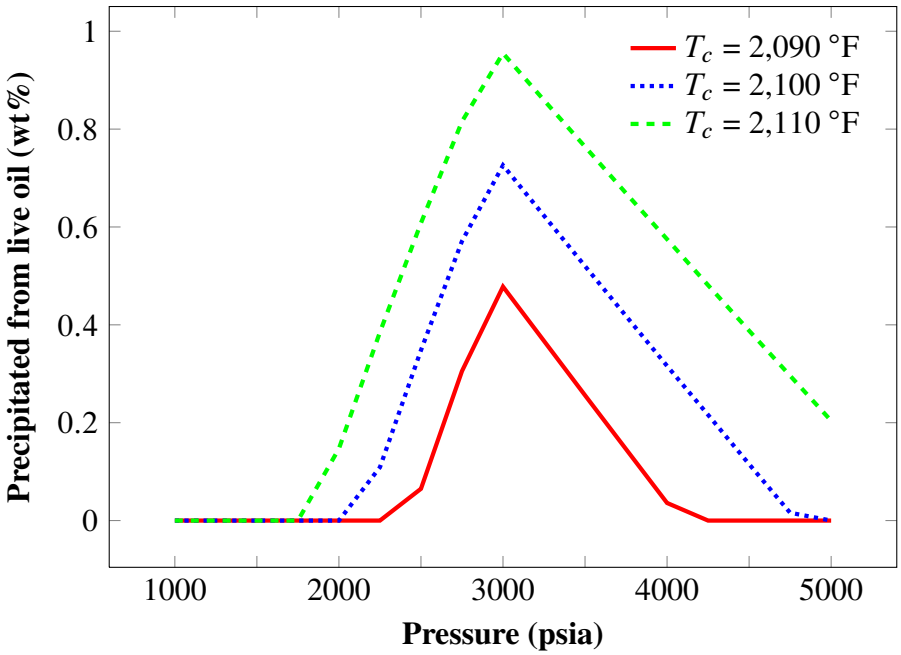

Fig. 4.7—Sensitivity analysis for T_c of the asphaltene component using 2,090 °F, 2,100 °F, and 2,110 °F. As the critical temperature increases, asphaltene precipitation increases and bubble point pressure decreases.

TABLE 4.9—ASPHALTENE PROPERTIES USED FOR CRITICAL TEMPERATURE SENSITIVITY ANALYSIS USING OIL 1 WHERE X REPRESENTS THE PARAMETER EVALUATED

Component	**Mw**	**Pc (psia)**	**Tc (F)**	ω
$Asphaltene$	800	178.3	**X**	1.441
Binary Interaction Coefficient				
$Asphaltene-$ light components (C_1 to C_5)	0.135			

4.2.3 Acentric factor (ω)

The impact of the acentric factor in the overall asphaltene precipitation was evaluated by varying its characterization with the following values: 1.45, 1.50, and 1.55. The fluid properties used are shown in **Table 4.10**. The results are shown in **Fig. 4.8**, suggesting that

increasing acentric factor reduces bubble point pressure and increases asphaltene precipitation as well as the pressure ranges where asphaltene precipitation is observed.

TABLE 4.10—ASPHALTENE PROPERTIES USED FOR ACENTRIC FACTOR SENSITIVITY ANALYSIS USING OIL 1 WHERE X REPRESENTS THE PARAMETER EVALUATED

Component	**Mw**	**Pc (psia)**	**Tc (F)**	ω
Asphaltene	800	178.2	2,105	**X**

Binary Interaction Coefficient

Asphaltene− light components (C_1 to C_5)	0.135

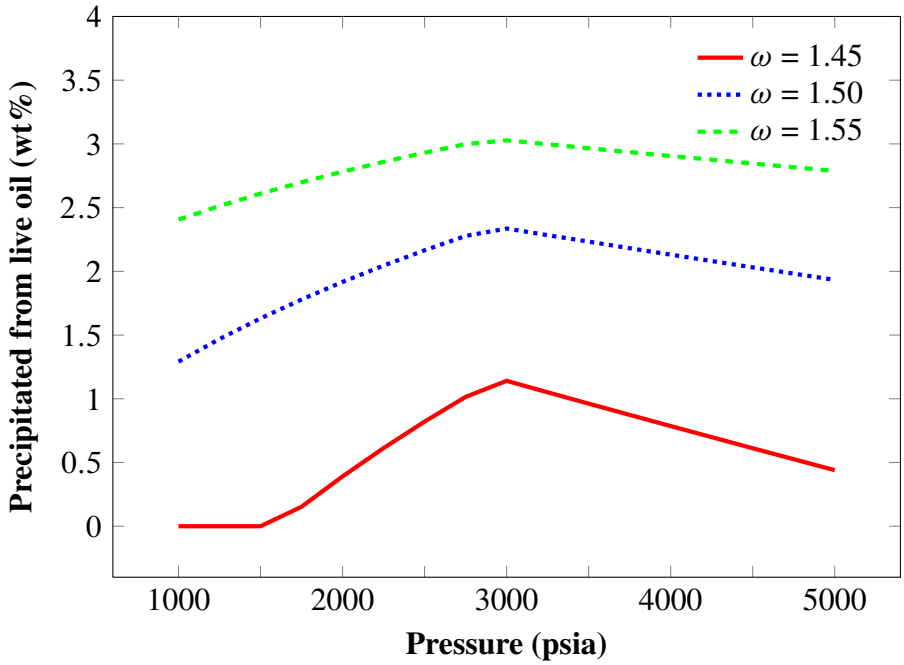

Fig. 4.8—Sensitivity analysis for ω of the asphaltene component using 1.45, 1.50, and 1.55. As acentric factor increases, asphaltene precipitation increases and bubble point pressure decreases.

4.2.4 Binary interaction coefficient

The binary interaction coefficients (BIC) between asphaltene and light components (C_1 to C_5) were evaluated using: 0.13, 0.15, and 0.17. For every case analyzed, the BIC is constant and equal for all light components. All other BIC were set to zero.

The full description of the asphaltene properties are shown in **Table 4.11**. The results of the evaluation are shown in **Fig. 4.9** where it's possible to observe that increasing BIC, increases asphaltene precipitation as well as modifying the symmetric shape of the precipitation envelope. The bubble point pressure also decreases as binary interaction coefficient increases.

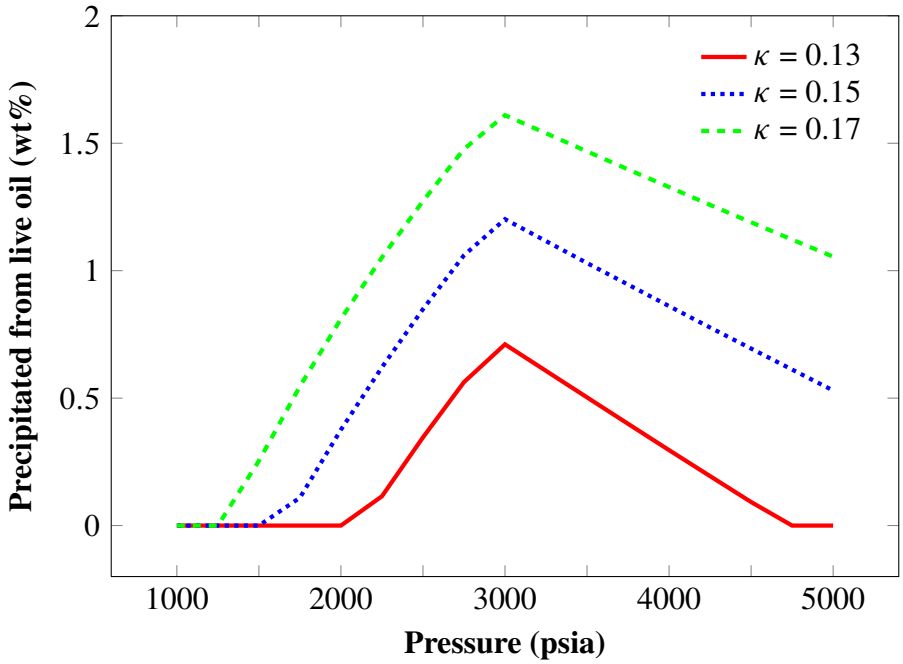

Fig. 4.9—Sensitivity analysis for κ of the asphaltene component and the lighter components (C_1 to C_5) using 0.13, 0.15, and 0.17. As the binary interaction coefficient increases, asphaltene precipitation increases as well as the bubble point pressure of the mixture.

TABLE 4.11—ASPHALTENE PROPERTIES USED FOR BINARY INTERACTION COEFFICIENT SENSITIVITY ANALYSIS USING OIL 1 WHERE X REPRESENTS THE PARAMETER EVALUATED

Component	**Mw**	**Pc (psia)**	**Tc (F)**	ω
$Asphaltene$	800	178.2	2,105	1.441

Binary Interaction Coefficient

$Asphaltene-$ light components (C_1 to C_5) **X**

4.3 Computational performance

In order to evaluate the computational time of the algorithm, we performed two analyses. The first one compares the three-phase (VLLE) and the two-phase (VLE) flashes in order to estimate the additional computer cost to include asphaltene in the simulation analyses. The second one compares the three-phase flash using vapor/liquid/dense-liquid and vapor/liquid/solid models. For each case, 45 cases were analyzed using different fluid compositions, pressures, and temperatures.

The studies were carried out in a personal computer with Intel Core 2 CPU processor, 6600 @ 2,40 GHz, 4.00 GB memory, and Windows 7 32-bits. The running time was calculated using a high-resolution counter that records the tick counts before and after executing the program and the tick frequency (ticks/sec).

The analysis were performed using Oil 1 (Table 4.4) and Oil 2 at different solvent concentrations (Table 4.5). Depending on the fluid conditions, pressures ranges from 200 psia to 3,300 psia, resulting in systems with one, two, or three phases.

4.3.1 Comparison of 2-phase and 3-phase flash

The VLLE flash algorithm requires higher CPU time as it performs additional calculations compared to a conventional VLE flash. The net increment in running time for a single VLLE point can be used as an estimate on the increment of a full-field numerical reservoir simulation run. This is very important as the flash calculation is repeated multiple times during a reservoir simulation, accounting for the majority of the CPU time. **Fig. 4.10** shows a graphic representation of the running time.

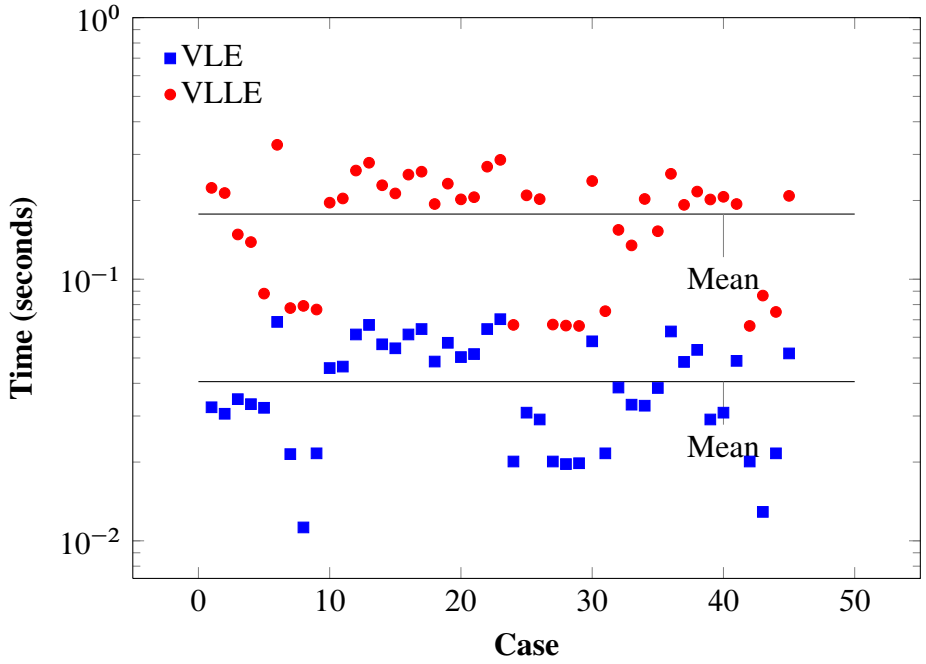

Fig. 4.10—Running time of VLE and VLLE flashes from 45 cases at different pressure and temperature conditions shows an increment of about 4.47 more time to execute a three-phase flash.

Table 4.12 shows the average, median, standard deviation, and minimum and maximum time of executing VLE and VLLE flashes. The three-phase flash takes 4.4 times longer to run compared to a conventional two-phase calculation. This can also be observed graphically in **Fig. 4.11**. A detailed table with the results obtained is shown in **Table 4.14**.

TABLE 4.12—STATISTIC COMPARISON BETWEEN CPU TIME SPENT TO CALCULATE VLE AND VLLE

Statistical functions	Time VLE (seconds)	Time VLLE (seconds)	Execution Ratio
Mean	0.0406	0.1775	1:4.47
Median	0.0384	0.2020	1:4.05
Standard Deviation	0.0170	0.0729	1:1.22
Minimum	0.0112	0.0663	1:2.73
Maximum	0.0703	0.3265	1:7.03

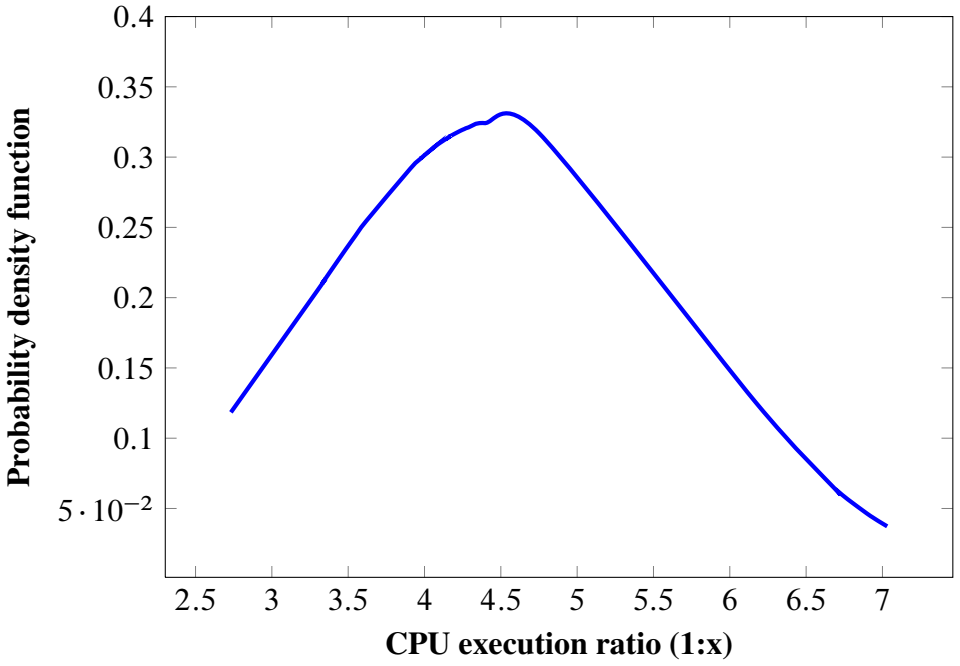

Fig. 4.11—CPU execution ratio VLLE-VLE follows a normal distribution, with an average mean of 4.47 times greater for VLLE calculations compared with VLE. The analyses was done using 45 fluids with different composition, pressure, and temperatures.

4.3.2 Comparison of dense-liquid and solid model flash

A comparison between the two main asphaltene precipitation models was performed. Both approaches require the calculation of a three-phase equilibrium, where the vapor/liquid/liquid flash was calculated using our algorithm as described in Chapter III, and the vapor/liquid/solid

model as it was outlined in Chapter II. For an unbiased comparison, we used the same fluid characterization for both models. This included the input parameters of the solid fraction: precipitation pressure, fugacity of the asphaltene fraction, and molar solid volume calculated using the cubic equation of state of a pure component. This results in nearly identical phase behavior calculations.

Fig. 4.12 shows the normal distribution of the time required to calculate the flash for the 45 cases. The running time of the two models exhibit a very similar probability distribution, just slightly shifted. In average, the dense-liquid model requires 1.1 more times to execute compared with the solid model, as shown in **Table 4.13**. The small incremental cost brings more reliable and stable phase behavior precipitations, accounting for the changes in pressure and composition.

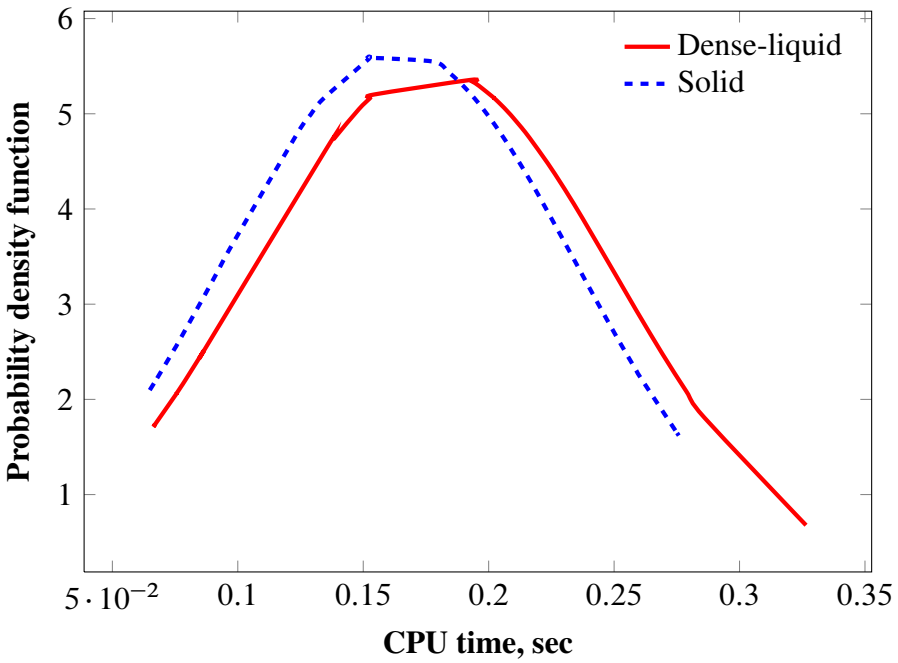

Fig. 4.12—Normal distribution of the CPU time for 45 cases showing that the dense-liquid model has a very similar computational time compared with the solid model.

TABLE 4.13—STATISTIC COMPARISON BETWEEN CPU TIME SPENT TO CALCULATE A FLASH WITH DENSE-LIQUID AND SOLID MODELS

Statistical functions	Solid (seconds)	Dense-liquid (seconds)	Execution Ratio
Mean	0.1643	0.1775	1:1.10
Median	0.1918	0.2020	1:1.04
Standard Deviation	0.0706	0.0729	1:0.18
Minimum	0.0649	0.0663	1:0.98
Maximum	0.2751	0.3265	1:1.73

TABLE 4.14—TIME TO RUN VLE AND VLLE FLASHES AT DIFFERENT PRESSURES AND TEMPERATURES USING FLUIDS FROM TABLES 4.1 AND TABLE 4.5

Case	Fluid	Pressure (psia)	Temp (°F)	2-phase (seconds)	Dense-liquid (seconds)	Solid (seconds)
1	Oil 1	2700	230	0.0306	0.2136	0.1235
2	Oil 1	2900	230	0.0324	0.2235	0.129
3	Oil 1	3100	230	0.03225	0.0881	0.0679
4	Oil 1	3300	230	0.01125	0.0791	0.0674
5	Oil 1	2000	212	0.0291	0.2018	0.2019
6	Oil 1	2200	212	0.0291	0.2024	0.1965
7	Oil 1	2400	212	0.0309	0.2066	0.207
8	Oil 1	2600	212	0.0309	0.2093	0.2031
9	Oil 1	2800	212	0.03285	0.2027	0.2016
10	Oil 1	3000	212	0.0129	0.0866	0.087
11	Oil 2	200	218	0.03315	0.1347	0.1339
12	Oil 2	400	218	0.03855	0.1544	0.1534
13	Oil 2	600	218	0.0384	0.1526	0.1518
14	Oil 2	800	218	0.0216	0.0755	0.075
15	Oil 2	1000	218	0.0201	0.0663	0.0666
16	Oil 2	200	250	0.0333	0.1387	0.0922
17	Oil 2	400	250	0.0348	0.1483	0.0978
18	Oil 2	800	250	0.0216	0.0766	0.0665
19	Oil 2	1000	250	0.02145	0.0776	0.0658
20	Oil 2 + 20%	1400	218	0.04635	0.2036	0.1878
21	Oil 2 + 20%	1600	218	0.0216	0.075	0.0763
22	Oil 2 + 20%	1800	218	0.0198	0.0663	0.0651
23	Oil 2 + 20%	2000	218	0.0201	0.0669	0.0649
24	Oil 2 + 20%	2200	218	0.01965	0.0665	0.065
25	Oil 2 + 20%	2400	218	0.0201	0.0671	0.0655
26	Oil 2 + 50%	1200	218	0.0504	0.202	0.1921

TABLE 4.14—CONTINUED

Case	Fluid	Pressure (psia)	Temp (°F)	2-phase (seconds)	Dense-liquid (seconds)	Solid (seconds)
27	Oil 2 + 50%	1400	218	0.0483	0.1925	0.1918
28	Oil 2 + 50%	1600	218	0.05205	0.2083	0.212
29	Oil 2 + 50%	1800	218	0.0537	0.2163	0.2161
30	Oil 2 + 50%	2000	218	0.05715	0.2319	0.22
31	Oil 2 + 50%	2400	218	0.0645	0.2577	0.2439
32	Oil 2 + 70%	1000	218	0.04575	0.1962	0.178
33	Oil 2 + 70%	1200	218	0.04845	0.1939	0.1838
34	Oil 2 + 70%	1400	218	0.05445	0.2128	0.2002
35	Oil 2 + 70%	1800	218	0.0579	0.2374	0.2334
36	Oil 2 + 70%	2000	218	0.0615	0.2603	0.2435
37	Oil 2 + 70%	2200	218	0.0645	0.2693	0.2589
38	Oil 2 + 70%	2400	218	0.07035	0.286	0.2751
39	Oil 2 + 78%	1200	218	0.04875	0.1939	0.1946
40	Oil 2 + 78%	1400	218	0.05175	0.2059	0.1972
41	Oil 2 + 78%	1600	218	0.0564	0.2287	0.2143
42	Oil 2 + 78%	1800	218	0.0615	0.2511	0.2374
43	Oil 2 + 78%	2000	218	0.06315	0.2529	0.2516
44	Oil 2 + 78%	2200	218	0.0669	0.2788	0.261
45	Oil 2 + 78%	2400	218	0.0687	0.3265	0.2749

CHAPTER V
SIMULATOR MATHEMATICAL FORMULATION

This chapter presents the mathematic formulation of a 3D fully compositional reservoir simulator built to predict asphaltene precipitation and deposition using VLLE. It describes the three governing equations: conservation of moles, conservation of volume, and equation of state. These expressions combined with auxiliary relations (well index, capillary pressure, viscosity, and damage due to asphaltene) define the flow in porous media of a multi-component reservoir with precipitation of asphaltene. The equations were discretized using finite differences and solved using a implicit-pressure, explicit-composition, and explicit-saturations method (IMPESC). The algorithm was implemented in MATLAB®.

5.1 Formulation assumptions

The general assumptions taken during the development of the numerical reservoir simulator are:

1. Finite difference discretization.
2. Block-centered grid geometry.
3. Isothermal system.
4. Steady-state during a timestep calculation.
5. Multiphase and multi-component flow described by Darcy's Law.
6. Instantaneous thermodynamic equilibrium represented by Peng-Robinson EOS in a three-phase (vapor, liquid, and solid) system.
7. No flow boundary condition.
8. Wells are described with Peaceman's model.
9. Rock is slightly compressible and immobile.
10. No chemical reactions or adsorption is considered.

11. Asphaltene is immobile and its precipitation is irreversible.

12. No water is found in the system.

5.2 Governing equations

5.2.1 Conservation of moles

The conservation of moles describes the relationship between the inflow and outflow of moles in a closed system in the absence of chemical reactions (Eq. 5.1). In this formulation, the moles of i leaving the system are considered as positive flow, while the moles entering as negative flow. Injection wells are accounted as negative flow.

$$\begin{Bmatrix}\text{Moles of } i\\ \text{accumulated}\end{Bmatrix} = \begin{Bmatrix}\text{Moles}\\ \text{of } i \text{ out}\end{Bmatrix} - \begin{Bmatrix}\text{Moles}\\ \text{of } i \text{ in}\end{Bmatrix} + \begin{Bmatrix}\text{Moles}\\ \text{of } i \text{ produced}\end{Bmatrix} - \begin{Bmatrix}\text{Moles}\\ \text{of } i \text{ injected}\end{Bmatrix} \tag{5.1}$$

The amount of moles of component i accumulated in a gridblock during a timestep (Δt) is the difference of moles in place between times n and $n+1$.

$$\begin{Bmatrix}\text{Moles of } i\\ \text{accumulated}\end{Bmatrix} = \frac{1}{\Delta t}\left(N_i^{n+1} - N_i^n\right) \tag{5.2}$$

For a multi-component reservoir simulation, Eq. 5.1 is written for every component ($i = 1, 2, ..., N_c$) in each phase ($\ell = 1, 2, ..., N_p$). In a 3D finite-difference model, the mole balance of a block (C) is represented by flow coming from or leaving to adjacent blocks: east (E), west (W), north (N), south (S), top (T), and bottom (B) as shown in Eq. 5.3.

$$\sum_{\ell=1}^{N_p}\left(q_{i\,E} + q_{i\,W} + q_{i\,N} + q_{i\,S} + q_{i\,T} + q_{i\,B} + q_{i_{inj/prod}}\right) = \frac{1}{\Delta t}\left(N_i^{n+1} - N_i^n\right) \tag{5.3}$$

The molar rate q_i can be expressed using Darcy's equation as shown in Eq. 5.4, where Q is the volume flow rate, ρ_m is the molar density, x_i is the molar composition, k is the absolute permeability, k_r is the relative permeability, μ is the viscosity, A is the flow cross-sectional area, ΔL is the distance between the center of the gridblock and the center of its neighboring block, and $\Delta\Phi^{n+1}$ is the difference of flow potentials (Eq. 5.20) of phase ℓ between the adjacent blocks. The calculation of viscosity is explained in section 5.3.3.

$$q_i = \sum_{\ell=1}^{Np} \left(Q \rho_m x_i \right)_\ell = \sum_{\ell=1}^{Np} \left(\frac{\rho_m x_i k_r k A}{\mu \Delta L} \Delta\Phi^{n+1} \right)_\ell \tag{5.4}$$

From Eq. 5.4, we can define flow coefficients for every component between center and its adjacent block. As an example, flow between center and east is shown in Eq. 5.5, where k is calculated using harmonic average, ρ_m and μ using arithmetic average, and k_r and x_i using the upstream cell property.

$$a_{i_{\ell,E}} = \sum_{\ell=1}^{Np} \left(\frac{\rho_m x_i k_r k A}{\mu \Delta L} \right)_\ell \tag{5.5}$$

Considering all neighboring cells, the total flow for component i can be written as:

$$\begin{aligned} \sum_{\ell=1}^{Np} \Delta a_{i_\ell} \Delta\Phi_\ell^{n+1} \quad = \quad & \sum_{\ell=1}^{Np} a_{i_{\ell,E}} \left(\Phi_{\ell,C}^{n+1} - \Phi_{\ell,E}^{n+1} \right) + \sum_{\ell=1}^{Np} a_{i_{\ell,W}} \left(\Phi_{\ell,C}^{n+1} - \Phi_{\ell,W}^{n+1} \right) \\ & \sum_{\ell=1}^{Np} a_{i_{\ell,N}} \left(\Phi_{\ell,C}^{n+1} - \Phi_{\ell,N}^{n+1} \right) + \sum_{\ell=1}^{Np} a_{i_{\ell,S}} \left(\Phi_{\ell,C}^{n+1} - \Phi_{\ell,S}^{n+1} \right) \\ & \sum_{\ell=1}^{Np} a_{i_{\ell,T}} \left(\Phi_{\ell,C}^{n+1} - \Phi_{\ell,T}^{n+1} \right) + \sum_{\ell=1}^{Np} a_{i_{\ell,B}} \left(\Phi_{\ell,C}^{n+1} - \Phi_{\ell,B}^{n+1} \right) \end{aligned} \tag{5.6}$$

Re-writing Eq. 5.3 using the flow coefficients, we have:

$$\sum_{\ell=1}^{Np} \left(\Delta a_i \Delta\Phi^{n+1} \right)_\ell + q_{i_{inj/prod}} = \frac{1}{\Delta t} \left(N_i^{n+1} - N_i^n \right) \tag{5.7}$$

5.2.2 Conservation of volume

Conservation of volume states that pore space is always completely filled by the total volume of fluids. It is expressed mathematically in Eq. 5.8, where V_t is the total volume, function of pressure and composition; and V_p is the pore volume, depending on pressure only.

$$V_t = V_p \tag{5.8}$$

Differentiating Eq. 5.8 with respect to time results in Eq. 5.9.

$$\left(\frac{\partial V_t}{\partial p}\right)_{\vec{N}} \frac{\partial p}{\partial t} + \sum_{i=1}^{N_c} \left[\left(\frac{\partial V_t}{\partial N_i}\right)_p \left(\frac{\partial N_i}{\partial t}\right) \right] = \frac{dV_p}{dp} \frac{\partial p}{\partial t} \tag{5.9}$$

If we assumed the formation to be slightly incompressible, then we can established the following relationship, where V_p^{ref} is the pore volume at reference pressure and c_f is the rock compressibility.

$$\frac{dV_p}{dp} = V_p^{ref} c_f \tag{5.10}$$

On the other hand, the change in total volume per each mole added of i is defined as the partial molar volume of the component (Eq. 5.11). For a finite-difference model, $\overline{V}_{iC}$ uses the upstream grid property. The derivation of the partial molar volume is described in Appendix A.

$$\overline{V}_{iC} = \left(\frac{\partial V_t}{\partial N_i}\right)_{p,T,N_{j\neq i}} \tag{5.11}$$

Replacing Eq. 5.10 and Eq. 5.11 into Eq. 5.9, and re-arranging the terms, we have:

$$\sum_{i=1}^{N_c} \left[\overline{V}_{iC} \left(\frac{\partial N_i}{\partial t}\right) \right] = \left[V_p^{ref} c_f - \left(\frac{\partial V_t}{\partial p}\right)_{\vec{N}} \right] \frac{\partial p}{\partial t} \tag{5.12}$$

The term V_{oid_C} can be defined from Eq. 5.12 to simplify and obtain Eq. 5.14.

$$V_{oid_C} = V_p^{ref} c_f - \left(\frac{\partial V_t}{\partial p}\right)_{\vec{N}} \tag{5.13}$$

$$\sum_{i=1}^{N_c} \left[\overline{V}_{i_C} \left(\frac{\partial N_i}{\partial t} \right) \right] = V_{oid_C} \frac{\partial p}{\partial t} \tag{5.14}$$

Differentiating Eq. 5.14 with respect to time using backward discretization, it yields the following expression:

$$\sum_{i=1}^{N_c} \left[\overline{V}_{i_C} \left(\frac{N_{i_C}^{n+1} - N_{i_C}^{n}}{\Delta t} \right) \right] = V_{oid_C} \left(\frac{p_C^{n+1} - p_C^{n}}{\Delta t} \right) \tag{5.15}$$

Combining the mole balance (Eq. 5.7) and the volume balance equations (Eq. 5.15) to satisfy both constraints simultaneously, results in Eq. 5.16.

$$\sum_{i=1}^{N_c} \left[\overline{V}_{i_C} \sum_{\ell=1}^{Np} \left(\Delta a_i \Delta \Phi^{n+1} \right)_\ell + q_{i_{inj/prod}} \right] = \frac{1}{\Delta t} V_{oid_C} \left(p_C^{n+1} - p_C^{n} \right) \tag{5.16}$$

5.2.3 Equation of state

The fluid behavior is modeled using Peng-Robinson EOS assuming instantaneous thermodynamic equilibrium within each time step. The fluid properties are calculated using the three-phase flash model described in Chapter III.

5.3 Auxiliary equations

The following auxiliary expressions are used in combination with the governing equations to define the reservoir simulation model.

5.3.1 Peaceman's well model

The well index is represented by Peaceman's well model (1978; 1983). The equation was derived to correct the bottomhole flowing pressure accounting for the difference in dimensions between the wellbore radius and the gridblock.

The model introduces the concept of equivalent radius of a well, the radius at which the steady-state flowing pressure for the actual well is equal to the numerically calculated pressure for the wellblock (Peaceman, 1978). For a nonsquare grid with anisotropic distribution of permeabilities, the equivalent radius of a wellblock r_o is calculated with Eq. 5.17.

$$r_o = 0.28 \frac{\sqrt{\sqrt{\frac{k_y}{k_x}}\Delta x^2 + \sqrt{\frac{k_x}{k_y}}\Delta y^2}}{\sqrt[4]{\frac{k_y}{k_x}} + \sqrt[4]{\frac{k_x}{k_y}}} \tag{5.17}$$

The production/injection molar rate of component i is calculated with Eq. 5.18. The difference between the block pressure and the bottomhole flowing pressure will determine if the well is injecting ($p_{wf} > p_C$) or producing ($p_C > p_{wf}$). For a production well, the fluid composition is the one in the well gridcell. For an injection well, fluid composition is defined as an input by the user. In the simulator, wells can be defined by specifying either flow rate at standard conditions, or constant bottomhole flowing pressure.

$$\begin{aligned} q_{i_{inj/prod}} &= \sum_{\ell=1}^{Np} \left\{ \frac{2\pi \rho_{m\ell} x_{i_\ell} k_{r_\ell} \sqrt{k_x k_y} h}{\mu_\ell} \left[\ln\left(\frac{r_o}{r_w}\right) + Skin \right] \left(p_C^{n+1} - p_{wf}^{n+1} \right) \right\} \\ &= \sum_{\ell=1}^{Np} \left[\frac{\rho_{m\ell} x_{i_\ell} k_{r_\ell}}{\mu_\ell} WI \left(p_C^{n+1} - p_{wf}^{n+1} \right) \right] \\ &= \sum_{\ell=1}^{Np} \left[a_{i_\ell} WI \left(p_C^{n+1} - p_{wf}^{n+1} \right) \right] \end{aligned} \tag{5.18}$$

5.3.2 Capillary pressure

The capillary pressure describe the difference of pressure in the interface of two immiscible phases, a wetting and a non-wetting phase. In an oil and gas system we assume the oil as the wetting phase, therefore we have:

$$pc_{vl} = p_v - p_l \tag{5.19}$$

With the capillary pressure between oil and gas, we can describe the flow potentials between two adjacent blocks (e.g. central C and east E) using Eq. 5.20 and Eq. 5.21, where $\overline{\rho}$ is the average mass density, Δh is the difference of height between the blocks, and Δpc_{vl} is the difference in vapor-liquid capillary pressure between the blocks. In our case, asphaltene is considered an immobile phase with the same compressibility as the rock, therefore, the phase is not considered in the flow coefficient calculations.

$$\Delta\Phi_l^{n+1} = \Delta p_E^{n+1} + \overline{\rho}_l^{n+1}\Delta h_E \tag{5.20}$$

$$\Delta\Phi_v^{n+1} = \Delta p_E^{n+1} + \overline{\rho}_v^{n+1}\Delta h_E + \Delta pc_{vl}^{n+1} \tag{5.21}$$

To solve the system using the IMPESC procedure, we lagged average densities, capillary pressure differentials, flow coefficients, partial molar volume, and Void term (Eq. 5.13). Replacing the well flow rate (Eq. 5.18) and the difference of potentials (Eq. 5.20 - 5.21) into Eq. 5.16 we can represent flow of phase ℓ between blocks C and E as:

$$\begin{aligned}\sum_{i=1}^{N_c}\Bigg\{\overline{V}_{i_C\ell}^{n}\Bigg[&\Delta a_{il,E}^{n}\Delta p_E^{n+1} + \Delta a_{il,E}^{n}\overline{\rho}_l^{n}\Delta h_E + \Delta a_{iv,E}^{n}\Delta p_E^{n+1} + \Delta a_{iv,E}^{n}\overline{\rho}_v^{n}\Delta h_E \\ &+ \Delta a_{iv,E}^{n}\Delta pc_{vl,E}^{n} + \left(a_{i_\ell}WI\right)^n\left(p_C^{n+1} - p_{wf}^{n+1}\right)\Bigg]\Bigg\} = \frac{1}{\Delta t}{V_{oid_C}}^n\left(p_C^{n+1} - p_C^{n}\right)\end{aligned} \tag{5.22}$$

Solving for all unknown from time level $n+1$ on the left hand size and the known on the right hand size of the equation, we have Eq. 5.23 describing the general finite-difference equation for a compositional simulator.

$$- A_T^n p_T^{n+1} - A_S^n p_S^{n+1} - A_W^n p_W^{n+1} + A_C^n p_C^{n+1} - A_E^n p_E^{n+1} - A_N^n p_N^{n+1} - A_B^n p_B^{n+1} = b^n \tag{5.23}$$

$$A^n p^{n+1} = b^n \tag{5.24}$$

where:

$$A_{E,W,N,S,T,B}^n = \sum_{i=1}^{N_c} \left(\overline{V}_{i_C}^n \sum_{\ell=1}^{Np} \Delta a_{i\ell,E,W,N,S,T,B}^n \right) \tag{5.25}$$

$$\begin{aligned} A_C^n &= A_E^n + A_W^n + A_N^n + A_S^n + A_T^n + A_B^n \\ &\quad + \sum_{i=1}^{N_c} \left(\overline{V}_{i_C}^n \sum_{\ell=1}^{Np} a_{i_\ell} WI \right] - \frac{1}{\Delta t} V_{oid}{}_C^n \end{aligned} \tag{5.26}$$

$$\begin{aligned} b^n &= -\frac{1}{\Delta t} V_{oid}{}_C^n p_C^n + \sum_{i=1}^{N_c} \left(\overline{V}_{i_C}^n \sum_{\ell=1}^{Np} a_{i_\ell} WI \right) p_{wf} \\ &\quad - \sum_{i=1}^{N_c} \left[\overline{V}_{i_C}^n \sum_{\ell=1}^{Np} \left(\Delta a_{i\ell}^n \overline{\rho}_\ell^n \Delta h \right) \right] \\ &\quad - \sum_{i=1}^{N_c} \left(\overline{V}_{i_C}^n \Delta a_{iv}^n \Delta p c_{vl}^n \right) \end{aligned} \tag{5.27}$$

5.3.3 Viscosity calculations

Using the fluid properties from the phase behavior flash, viscosities of oil and gas are calculated using Eq. 5.28 proposed by Lohrenz et al. (1964). This empirical correlation uses the residual viscosity concept and the theory of the corresponding states, where μ_ℓ is the viscosity of the phase ℓ, μ_ℓ^* is the viscosity at atmospheric pressure of the phase ℓ, ζ_ℓ is the viscosity parameters of phase ℓ, and ρ_{mr_ℓ} is the reduced molar density of phase ℓ.

$$\begin{aligned}\mu_\ell =& \mu_\ell^* + \frac{1}{\zeta_\ell}\Big[\big(0.1023 + 0.023364\rho_{mr_\ell} + 0.058533{\rho_{mr_\ell}}^2 - 0.40758{\rho_{mr_\ell}}^3 \\ &+0.0093324{\rho_{mr_\ell}}^4\big)^4 - 0.0001\Big]\end{aligned} \tag{5.28}$$

The phase viscosity at atmospheric pressure μ_ℓ^* is calculated using Eq. 5.29, where μ_i^* is the viscosity of component i in the ℓ phase at low pressure and it's calculated using Eq. 5.30.

$$\mu_\ell^* = \frac{\sum z_i \mu_i^* \sqrt{M w_{i_\ell}}}{\sum z_i \sqrt{M w_{i_\ell}}} \tag{5.29}$$

$$\mu_i^* = \begin{cases} \dfrac{0.00034\left(T_{r_i}\right)^{0.94}}{\zeta_i}, & \text{if } T_{r_i} \leq 1.5 \\ \\ \dfrac{0.0001776\left(4.58T_{r_i} - 1.67\right)^{5/8}}{\zeta_i}, & \text{if } T_{r_i} > 1.5 \end{cases} \tag{5.30}$$

The reduced temperature of component i is denoted T_{r_i} and it is calculated using Eq. 5.31. The viscosity parameter ζ of component i is calculated with Eq. 5.32.

$$T_{r_i} = \frac{T}{\sum_{i=1}^{Nc} T_{c_i}} \tag{5.31}$$

$$\zeta_i = \frac{T_{c_i}^{1/6}}{M w_i^{1/2} P_{c_i}^{2/3}} \tag{5.32}$$

The phase viscosity parameter ζ_ℓ is calculated using Eq. 5.33, an expression similar to Eq. 5.32 but using the pseudo-properties for the mixture. T_{pc_ℓ} and P_{pc_ℓ} are calculated with Eq. 5.34 and Eq. 5.35 respectively, and the phase molecular weight $M w_\ell$ is calculated with Eq. 5.36.

$$\zeta_\ell = \frac{T_{pc_\ell}^{1/6}}{M w_\ell^{1/2} P_{pc_\ell}^{2/3}} \tag{5.33}$$

$$T_{pc_\ell} = \sum_{i=1}^{Nc} z_i T_{c_i} \tag{5.34}$$

$$P_{pc_\ell} = \sum_{i=1}^{Nc} z_i T_{c_i} \tag{5.35}$$

$$M w_\ell = \sum_{i=1}^{Nc} z_i M w_i \tag{5.36}$$

Finally, the reduced molar volume ρ_{mr_ℓ} of the phase is calculated with Eq. 5.37.

$$\rho_{mr_\ell} = \frac{\rho_\ell \sum_{i=1}^{Nc} z_i V_{c_i}}{M w_\ell} \tag{5.37}$$

5.3.4 Damage due to asphaltene precipitation

Once asphaltene precipitates from the live oil, it deposits in the rock porous reducing the pore space and the effective flow paths. The following section presents the models used for representing formation damage by reducing porosity and permeability.

Porosity reduction

To account for the reduction of pore volume due to asphaltene deposition, the gridblock porosity is updated as a function of solid saturation. This model accounts for the volume of asphaltene molecules (based on molar density) occupying and plugging the pore space. It assumes the entire pathway can be plugged by asphaltene and does not consider its flow once it has been precipitated as a solid phase.

Porosity after asphaltene has been deposited ϕ^{n+1} is calculated using Eq. 5.38 (Civan, 1992, 2000; Schlumberger, 2011; Vafai, 2005), where ϕ_0 is the initial porosity, and S_s is the volume fraction of asphaltene deposited.

$$\phi^{n+1} = \phi^n \left(1 - S_s^{n+1}\right) \tag{5.38}$$

Permeability reduction

Similar to porosity reduction, the effective flow paths are reduced when asphaltene deposits and plugs the pore throats. Gruesbeck (1982) suggest the use of the empirical correlations for porosity-permeability displayed in Eq. 5.39. α is a user-defined reduction parameter that can be used to calibrate the model and history match data.

$$\ln \frac{k}{k^{n+1}} = \left(\phi^n - \phi^{n+1}\right)^{\alpha} \tag{5.39}$$

Combining this equations with Eq. 5.38, we have the model to represent the reduction of permeability: Eq. 5.40.

$$k^{n+1} = \frac{k^n}{exp\left(\phi^n S_s^{n+1}\right)^{\alpha}} \tag{5.40}$$

The value of the permeability reduction parameter α is highly related to the average pore throat diameter. Small pores are more susceptible to plugging and reduction of flow space due to adsorption. α is a very important parameter as it determines the degree of reservoir

damage due to asphaltene precipitation. The value is usually used for matching the reservoir history, although it can also be obtained from experimental coreflood data. **Fig. 5.1** shows the impact on permeability as we varied α with an initial permeability of 10 mD and initial porosity of 0.2.

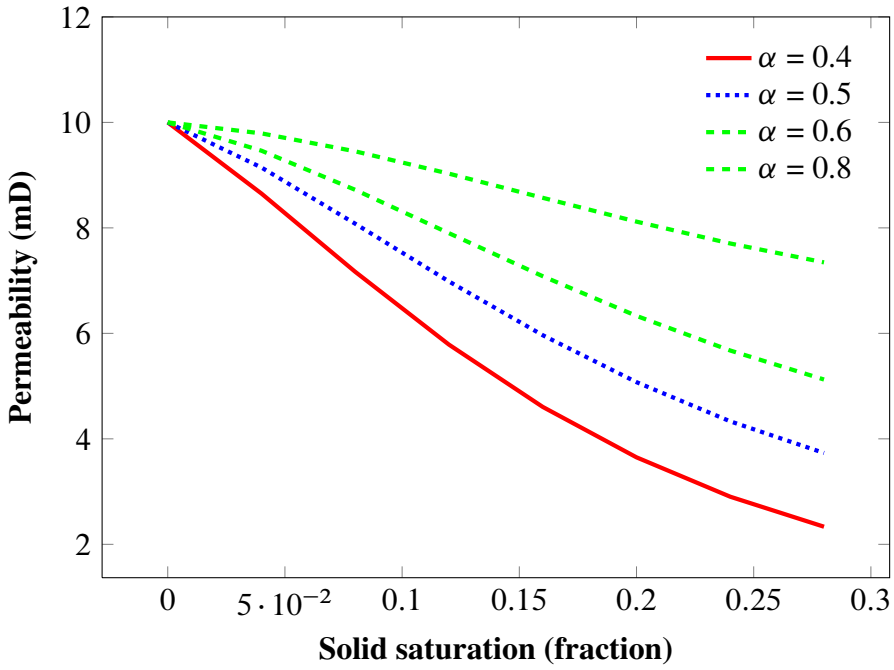

Fig. 5.1—Permeability reduction as a function of solid saturation for α values of 0.4, 0.5, 0.6, and 0.8.

5.4 Matrix solution

The general equation to solve a single gridblock in a compositional system is Eq. 5.23. There would as many equations as number of grid blocks in the model, allowing us to solve simultaneously the equations for all the grid blocks in the matrix form shown in Eq. 5.41.

$$A\underline{p} = b \tag{5.41}$$

Because matrix A from Eq. 5.41 is mainly populated by zeros, we can reduce the size of the matrix, and the storage requirement, by extracting all nonzero diagonals creating a sparse band and diagonal matrices. Two methods are included for solving the matrix: direct solution and preconditioned conjugate gradients method. It's important to notice that direct solutions require large storage memory, therefore it is usually reserved for small size problems.

The overall time step is solved using IMPESC method, previously developed by Acs et al. (1985), where the system of equations is solved similar to a black-oil model with pressures solved implicitly and compositions and molar densities solved explicitly. This involves evaluating A and b at the previous iteration k to solve the pressure for the next timestep p^{n+1}. Because we are lagging some parameters ($\overline{\rho}_\ell$, $\Delta pc_{v\ell}$, $\Delta a_{i\ell}$, $\overline{V}_{i_C\,\ell}$, V_{oid_C}) in the development of our equations that depend on the pressure solution, we performed an iteration procedure to correct for this approximation, where A and b are updated in each iteration and the process is repeated until the convergence criteria is reached.

To increase the computational efficiency of the algorithm, the following features were included to reduce the total CPU time.

Timestep control

When using IMPESC method, the non-linearity of the problem can result in the need of small time steps to preserve stability and accuracy. However, the optimal time discretization varies along the simulation study depending on the specific conditions. For example, early production or injection usually requires very small variation of time while steady flow can handle long time steps. For our algorithm, we specified the maximum number of

IMPESC iterations and the largest time step to be allowed. During the first timestep trial, we attempt to solve using the largest allowed with the methodology described previously. If the solution does not converge, the timestep would be reduced by half, or any percentage as defined by the user. In most cases, smaller time steps leads to smaller variations in the physical properties, therefore the iteration system is easier to solve.

Parallel processing

Using MATLABs built-in function for parallel processing, the nested loop calculating the thermodynamic properties was programmed to use multiple cores. The flash equilibrium calculation is performed for every cell as a function of known properties from the previous iteration. The independence between each cell allows dividing the model into smaller pieces (a defined number of gridcells) to carry out simultaneous calculations.

Restart

The restart option creates a new simulation run based on results from an existing case. The model is initialized using the variables stored during the original simulation, and continues the computations as requested in the new input data. It is possible to change the well scheduling data, maximum time step, maximum number of iterations, etc.

The steps for IMPESC are summarized below, where k is the iteration number and n is the result from the previous time step. This procedure is repeated in every time calculation.

1. For $k = 0$ and Δt set:
   - $p^k = p^n$
   - $\phi^k = \phi^n$
   - $k_x^k = k_x^n$
   - $k_y^k = k_y^n$
   - $k_z^k = k_z^n$

2. Perform a three-phase flash to calculate fluid properties at p^k.

3. Modify porosity and permeability using Eq. 5.38 and Eq. 5.40, using the result from p^k.

4. Calculate relative permeabilities and viscosities at p^k.

5. Calculate flow coefficients, partial molar volume, and Void at p^k.

6. Solve p^{k+1} from Eq. 5.23.

7. Calculate the total moles using Eq. 5.7.

8. Calculate the new fluid composition using Eq. 5.42.

$$Z_i^{n+1} = \frac{N_i^{n+1}}{\sum_{i=1}^{Nc} N_i^{n+1}} \tag{5.42}$$

9. Test if convergence criterion is achieved using $\epsilon \leq 1x10^{-3}$, where ϵ is given by Eq. 5.43, and if the iteration number k is less than maximum allowed.

$$\epsilon = max \left\{ \left| \frac{p^{k+1} - p^k}{p^k} \right| \right\} \tag{5.43}$$

10. If the criteria is met, then $p^n = p^{k+1}$ and Δt is incremented using Eq. 5.44. A maximum delta time is defined by the user (e.g. 30 days), after which Δt is not further incremented.

$$\Delta t = \Delta t + \frac{\Delta t}{2} \tag{5.44}$$

11. If the criteria is not met, then update $p^k = p^{k+1}$ and $k = k + 1$. Repeat steps 2 to 9 until convergence criterion are satisfied. If the iteration number is greater than the maximum allowed, then go to step 12.

12. Reduce the time step using Eq. 5.45 and repeat the procedure from step 1 using the information at n level. A minimum delta time is defined by the user (e.g. 0.01 days), after which Δt is not further reduced.

$$\Delta t = 0.5\Delta t \tag{5.45}$$

CHAPTER VI
RESERVOIR SIMULATION RESULTS

This chapter presents the results from several reservoir simulation runs performed to: a) Evaluate the phase behavior of asphaltene and deposition patterns within the reservoir and b) Assess the robustness and stability of the algorithm and its features. For all cases, we used oil 1 (see Chapter IV), grouped into 8 new components to reduce the CPU time. Two different geological models were analyzed: homogeneous, to understand the deposition mechanisms and investigate their physical behavior; and heterogeneous, representing a simplified fluvial environment to test the program under more realistic conditions where high rock property contrast is observed. The result shows four distinct stages in the asphaltene precipitation process, depending on the fluid behavior and formation damage level.

6.1 Mechanistic analysis

To understand the mechanisms of asphaltene precipitation, we analyzed the behavior of a homogeneous reservoir producing by natural depletion. The following sections describe the properties used in the model.

6.1.1 Model description

The reservoir is represented by a symmetrical block-centered 2D model with 625 cells (nx=25, ny=25, and nz=1) as shown in **Fig. 6.1**, where each gridcell measures 320ft by 320ft by 80ft. The model has a constant depth of 14,000 feet, without changes in the structure of the subsurface throughout the reservoir. It has an initial pressure of 5,500 psia and initial temperature of 212 °F. The model properties are:

Rock properties

Initially, the reservoir has a porosity of 16%, horizontal permeability of 10mD, and verti-

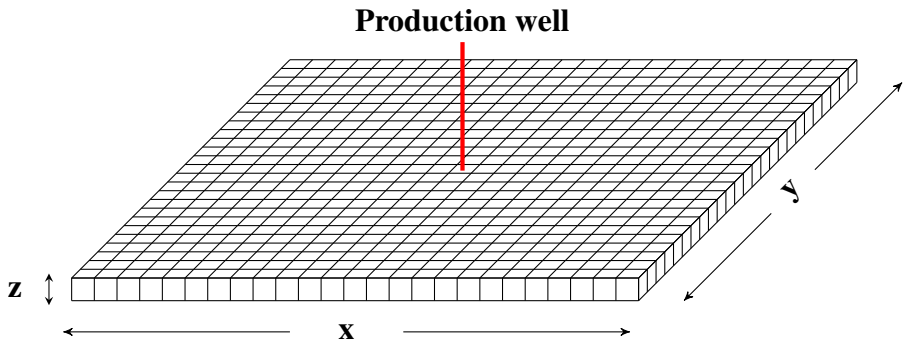

Fig. 6.1—2D reservoir simulation grid with 625 cells (nx=25, ny=25, and nz=1) used to study the mechanistics of asphaltene precipitation.

cal to horizontal permeability ratio of 0.1. Both porosity and permeability are considered dynamic properties changing with pressure (time) using the formation damage model previously described with a permeability reduction parameter (α) of 0.6. A full summary of the rock properties is shown in **Table 6.1**.

TABLE 6.1—ROCK PROPERTIES USED IN THE MECHANISTIC STUDY SIMULATION

Pressure	5,500	psia
Temperature	212	°F
Porosity	16	%
Horizontal permeability (mD)	10	mD
Kh/Kv	0.1	fraction
Top depth	14,000	feet
Reference pressure	3,600	psia
Rock compressibility	4×10^{-6}	1/psia
Permeability reduction parameter (α)	0.6	

Fluid characterization

We used oil 1 from Burke et al's experiments (Table 4.4). It has a bubble point pressure of 2,953 psia, exhibiting asphaltene precipitation from 2,000 psia to 5,159 psia, and reaching its maximum deposition at the bubble point pressure. At initial reservoir conditions (com-

position, pressure, and temperature), the fluid is found subsaturated and above the upper asphaltene onset pressure. At this point, only liquid phase exists in the system. As the pressure decreases, gas and solid are formed.

In order to reduce CPU time, the components were lumped from the original 12 into 8 new pseudo-components, following the constraints imposed by Eq. 6.1 and Eq. 6.2.

$$z_{grouped} = \sum_{i=1}^{N_{group}} z_i \qquad (6.1) \qquad Mw_{grouped} = \sum_{i=1}^{N_{group}} Mw_i z_i \qquad (6.2)$$

The grouping was done based on K-values (tendency of a component to partition itself between liquid and vapor phases), molecular weights, mole fraction, and preservation of binary interaction coefficients. It is important to notice that CO_2 was characterized as pure component to be later used in enhanced oil recovery studies. **Fig. 6.2** shows that the lumped fluid has a very similar prediction of asphaltene precipitation compared to the original 12-component characterization. The final fluid properties are shown in **Table 6.2**.

TABLE 6.2—FLUID PROPERTIES USED FOR OIL 1 GROUPED TO 8-COMPONENTS

Component	**MW**	**Pc (psia)**	**Tc (F)**	**Acentric Factor**	z_i **(%)**	Vc
CO_2	44.01	1,070.2	87.6	0.2250	2.46	1.505
$C_1 + N_2$	16.23	664.7	-118.7	0.0085	36.94	1.588
$C_2 + C_3$	37.59	658.6	152.1	0.1271	7.52	2.841
C_4	58.10	544.5	296.0	0.1878	1.93	4.126
C_5	72.20	490.2	377.5	0.2397	1.57	4.956
C_6	86.00	477.2	453.5	0.2750	1.62	5.917
$C_{7+}^{nonprec}$	320.0	180.8	1,089.0	1.022	47.145	26.0000
$Asphaltene$	800.00	178.3	2,105.0	1.441	0.815	60.717

Binary Interaction Coefficient

$Asphaltene-$ light components (C_1 to C_5)	0.135
$C_{7+}^{nonprec} - C_1$	0.053

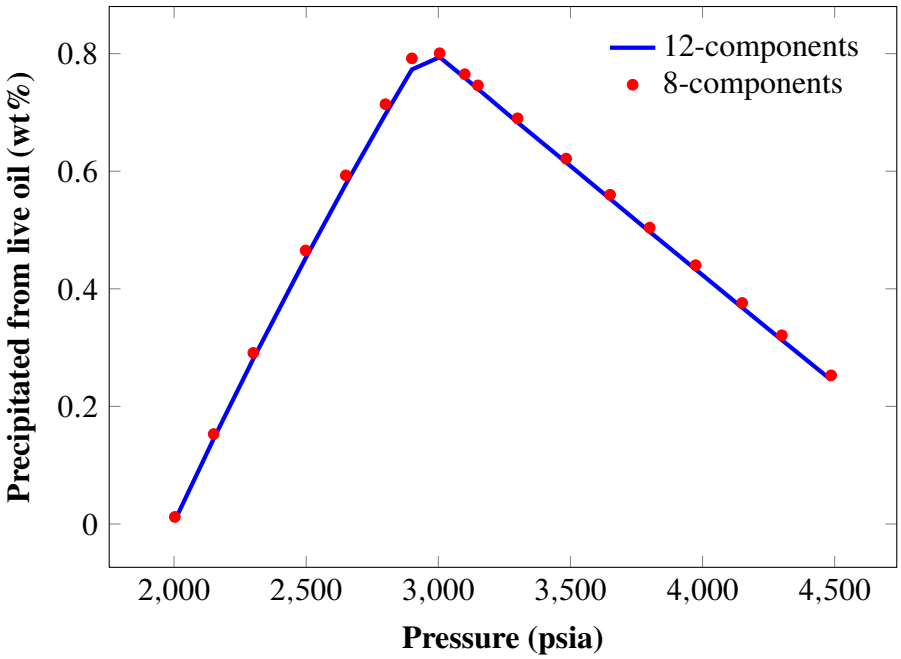

Fig. 6.2—Comparison of asphaltene precipitation using fluids with 12-component (original) and 8-components (grouped) shows there is no significant difference in the prediction results.

Fluid-rock properties

The fluid-rock properties model the dynamic properties of the rock as it interacts with the fluid at different reservoir conditions. First, relative permeabilities represent the relative movement of a phase during multi-phase flow. **Fig. 6.3** shows the relative permeability curves for oil and gas. As only liquid and gas are considered movable phases, we do not need to define any other relative permeability curve or a three-phase relative permeability model.

On the other hand, capillary pressures accounts for the difference in pressures between oil and gas across its interface. This definition was used in Chapter V during the mathematic derivation of a reservoir simulator. **Table 6.3** lists the relative permeabilities and capillary pressures with respect to gas saturation.

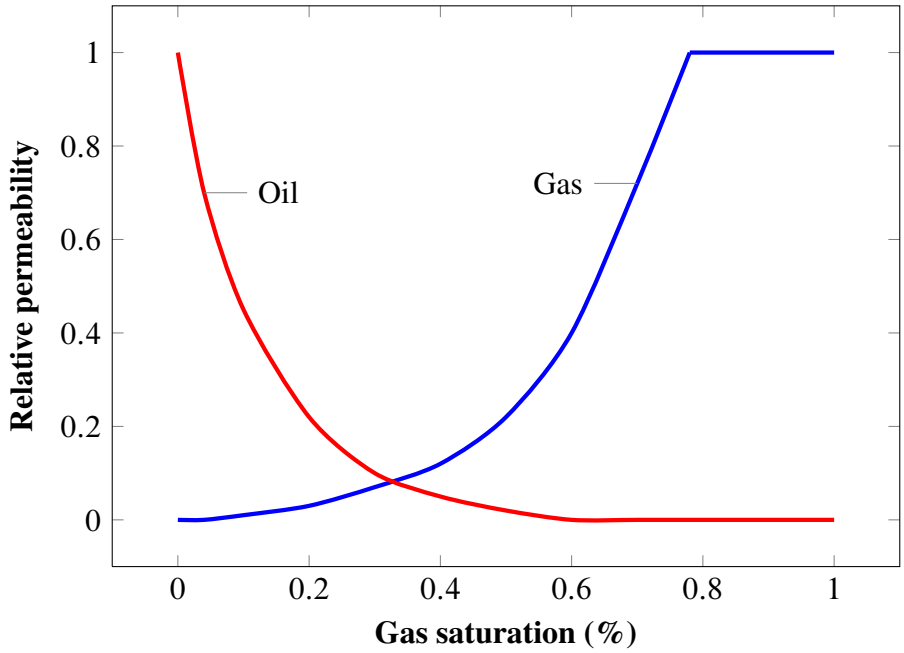

Fig. 6.3—Representative relative permeability curves for oil and gas which determines the relative flow when both phases are present in the system.

TABLE 6.3—RELATIVE PERMEABILITIES AND CAPILLARY PRESSURE OF OIL AND GAS

Sg	Krg	Kro	Pc
0	0	1	0
0.04	0	0.7	0.2
0.041	0.001	0.69	0.21
0.1	0.01	0.44	0.5
0.2	0.03	0.22	1
0.3	0.07	0.1	1.5
0.4	0.12	0.05	2
0.5	0.22	0.02	2.5
0.6	0.4	0	3
0.7	0.72	0	3.5
0.78	1	0	3.9
1	1	0	3.9

Well description

The model has a single producing well located in the center of the array. It has a wellbore radius of 0.75 feet and skin of zero; formation damage was considered only as a reduction of permeability due to asphaltene precipitation. The well was set to produce at a maximum oil production rate of 1,000 stb/day, with a lower limit for bottomhole flowing pressure of 2,000 psia. This means that the well would produce 1,000 stb/day of oil while the bottomhole flowing pressure is greater than 2,000 psia. Once the well cannot produce at the desired rate, it will be automatically changed to maintain a constant bottomhole flowing pressure.

6.1.2 Asphaltene precipitation process

The process of asphaltene precipitation from live-oils and its deposition in a reservoir can be divided into several stages. Depending on its initial conditions and its development program, a field may or not go through all these periods. Based on this mechanistic analysis, we can identify the following phases:

Stage 1: Reservoir pressure above upper AOP

During this period, asphaltene does not precipitate within the reservoir and no reduction of porosity or permeability occurs. However, precipitation of asphaltene in the wellbore may still occur, potentially causing obstruction of the production tubing and increasing the pressure drop in the well. Precipitation of asphaltene in the flowlines and surface facilities is not considered in this study.

Stage 2: Near wellbore pressure below upper AOP

Precipitation and deposition of asphaltene begins when a sector of the reservoir falls below the upper AOP (5,159 psia for this case). During this period, the only area affected by asphaltene precipitating is the wellbore region, where pressure is the lowest of the system. The rest of the reservoir remains undisturbed by changes in composition and no negative

effects are observed in the production performance compared to a case without asphaltene precipitation. **Fig. 6.4** depicts the pressure distribution after 210 days of production, showing pressures triggering asphaltene near the well. As a new solid phase is formed, the composition of the liquid phase changes accordingly. Less asphaltene results in liquid fractions with higher percentages of the lighter components, thus affecting the density and the viscosity. At 210 days of production, the area without asphaltene precipitation has a viscosity of 2.37 cp, compared to 2.32 at the wellbore.

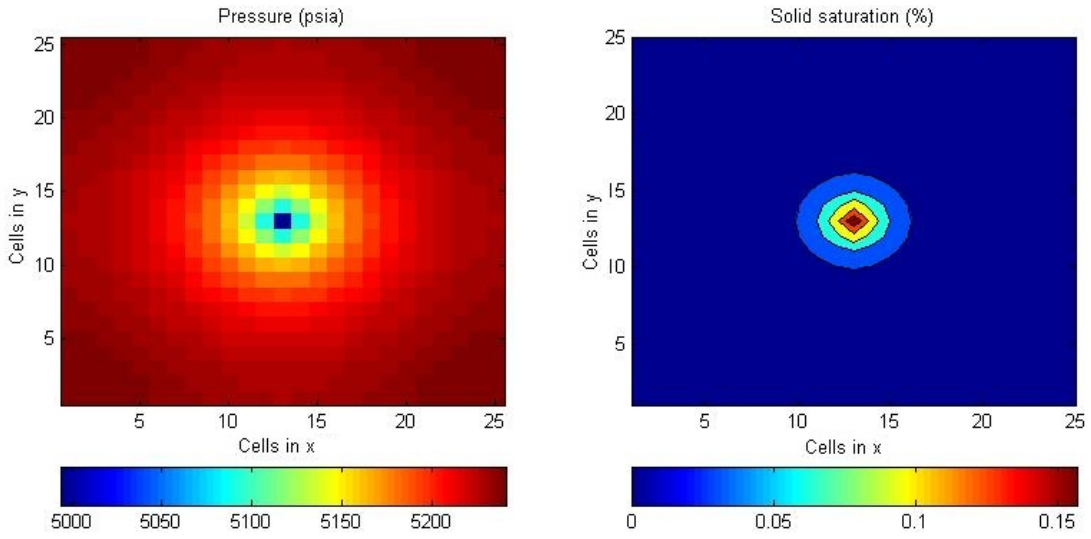

Fig. 6.4—Pressure distribution at 210 days (stage 2) of simulation shows lowest pressure near the wellbore, where the highest solid saturation is found.

Stage 3: Reservoir pressure below upper AOP

In this stage, the entire pressure falls below the AOP due to continuous fluid extraction triggering the deposition of asphaltene throughout the reservoir. For our case, after 540 days, average pressure is 4,747 psia, lower than the upper AOP of 5,159 psia. Pressure distribution and solid saturation in **Fig. 6.5** depicts deposition along the reservoir, with highest saturation in the wellbore. As we produce the reservoir, asphaltene continues to precipitate. Consequently, the oil reaching the well contains a smaller fraction of asphaltene and it does not require the formation of a solid phase to remain in equilibrium. Therefore, the

highest precipitation is found in the wellbore region, but not in the well vicinities as seen **Fig. 6.6**.

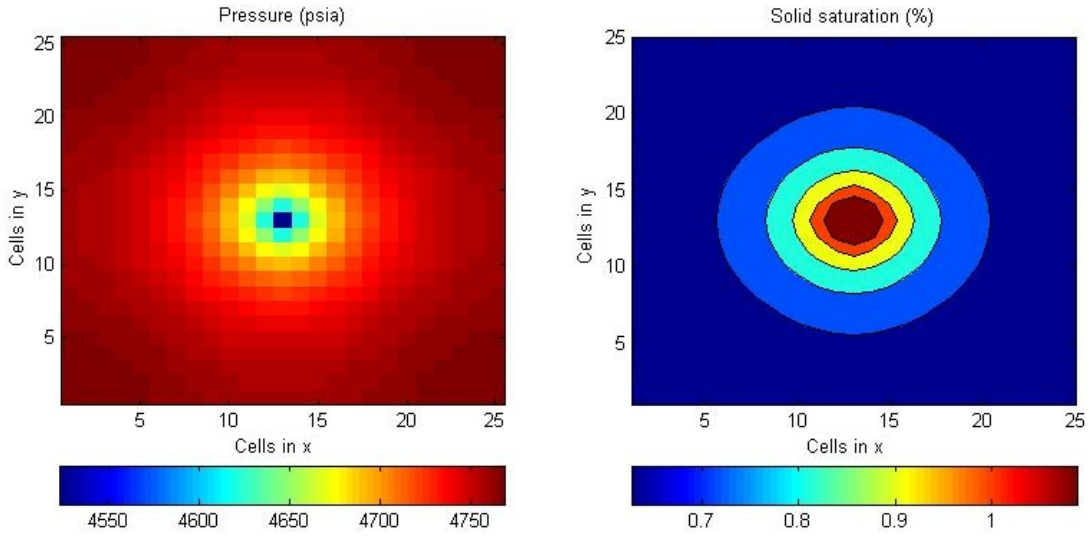

Fig. 6.5—Pressure distribution at 540 days (stage 3) of simulation shows entire reservoir below the upper AOP. Small amounts of asphaltene deposited along the entire reservoir. The highest precipitation is observed near the wellbore.

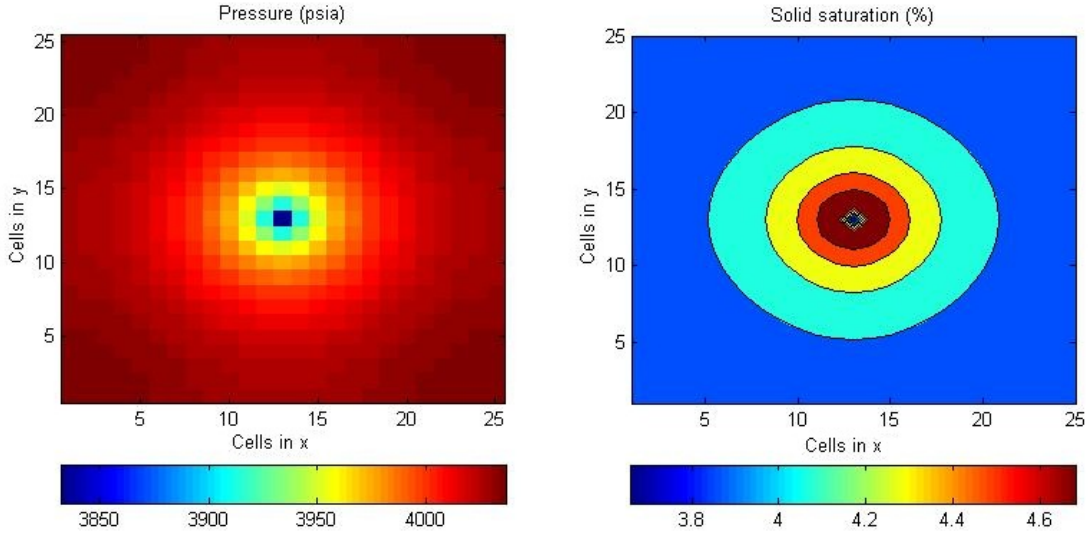

Fig. 6.6—Pressure distribution at 1,050 days (stage 3) of simulation shows the entire reservoir below the upper AOP, thus exhibiting asphaltene precipitation. The highest solid saturation is observed near the wellbore but not in its vicinities.

As we continue to produce the reservoir and lower the pressure, asphaltene would continue to deposit in the pore throats, reducing the reservoir permeability. The extend of the damage would depend on the size and tortuosity of the pore throat. In our mathematical model, this is controlled by the permeability reduction model and the permeability reduction parameter (α). For our case, horizontal permeability has reduced almost by 40% after 1,800 days of production with the pressure distribution shown in **Fig. 6.7**. The highest permeability reduction is observed in the wellbore region.

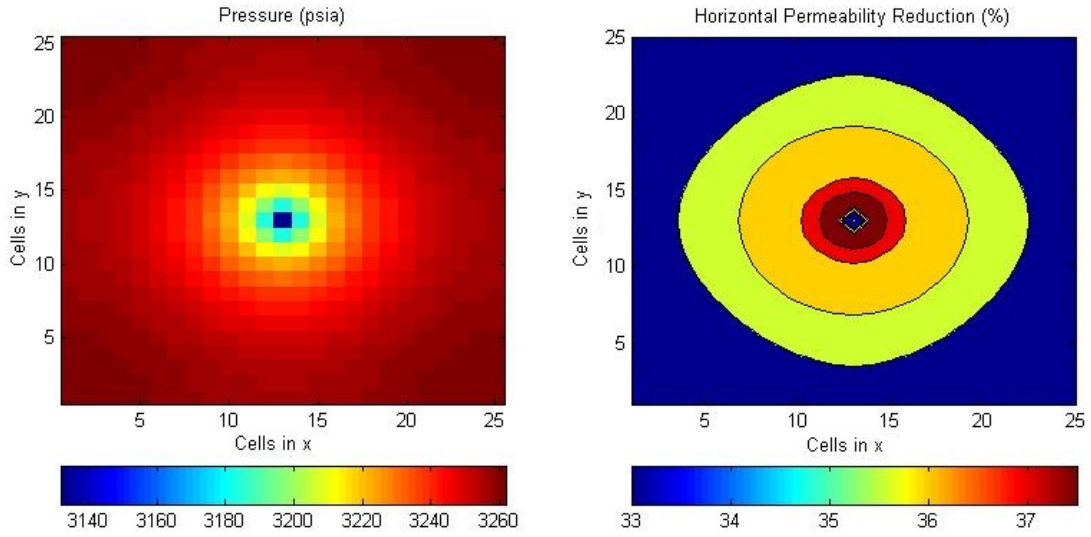

Fig. 6.7—Pressure distribution at 1,800 days showing average pressures of 3,065 psia. There is a permeability reduction (%) of almost 40%, with highest variation near the wellbore region.

The progressive reduction of permeability can be observed in **Fig. 6.8**. At 540 days of production, no significant reduction of permeability is observed. Starting from 1,050 days, permeability starts to decrease and reaches almost 40% reduction by 1,800 days. Once the reservoir reached this phase, the reservoir has suffered irreversible damage that will only increase as the reservoir continues production.

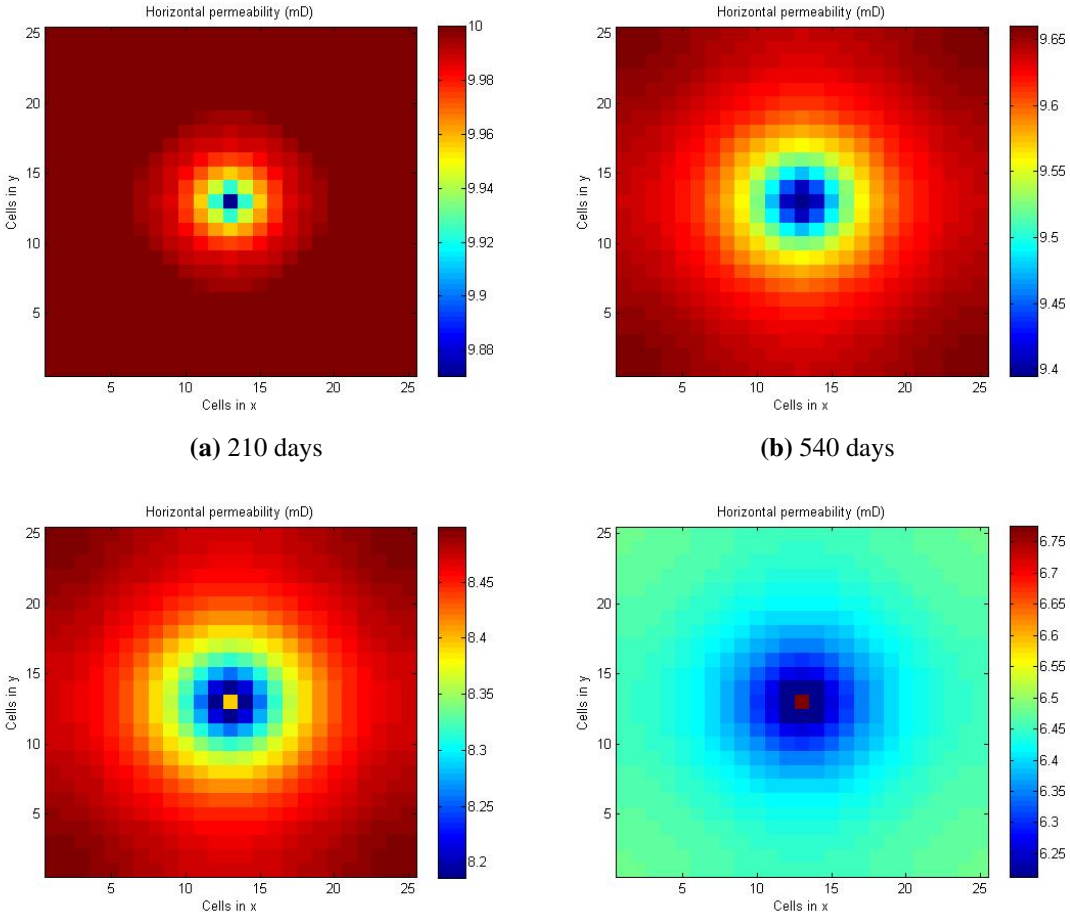

(a) 210 days **(b)** 540 days

(c) 1,050 days **(d)** 1,800 days

Fig. 6.8—Progressive reduction of permeability for a homogeneous case at 210, 540, 1050, and 1800 days of production. By 1,800 days, permeability is reduced by almost 40%.

Stage 4: Reduction in rate of precipitation

The final phase occurs when the rate of asphaltene precipitation is reduced. At this point, fluid composition contains very small fractions of asphaltene as a result of two reasons:

1. Significant amounts of asphaltene have already precipitated as a solid phase.
2. After the fluid reached the bubble point pressure, gas broke out of solution and asphaltene becomes more soluble in the liquid phase.

The transition from stages 3 and 4 is observed when analyzing the derivative of solid saturation with respect to time (**Fig. 6.10**). This period occurs as the first free gas is released from the liquid phase at 2,070 days. As the pressure continuous to decrease, the entire reservoir falls below the saturation pressure and asphaltene becomes more soluble in the liquid phase. At 2,100 days, the deposition rate changes.

From an economic point of view, the effect of asphaltene precipitation and permeability reduction can be magnified when comparing cumulative oil production with and without asphaltene precipitation. **Fig. 6.9** shows a difference of 13% after 3,000 days of production for the case evaluated. This difference illustrates the importance of properly modeling asphaltene precipitation in the reservoir as it allows more reliable production forecasts that can significantly impact the project economics and the reservoir development plan.

6.1.3 Permeability reduction parameter

A sensitivity analysis was performed to evaluate the effect of the permeability reduction parameter α on the overall asphaltene deposition. The scenarios considered were: 0.4, 0.5, 0.6, and 0.8. For this study, we used the reservoir and grid properties described in the mechanistic analysis section, only varying α.

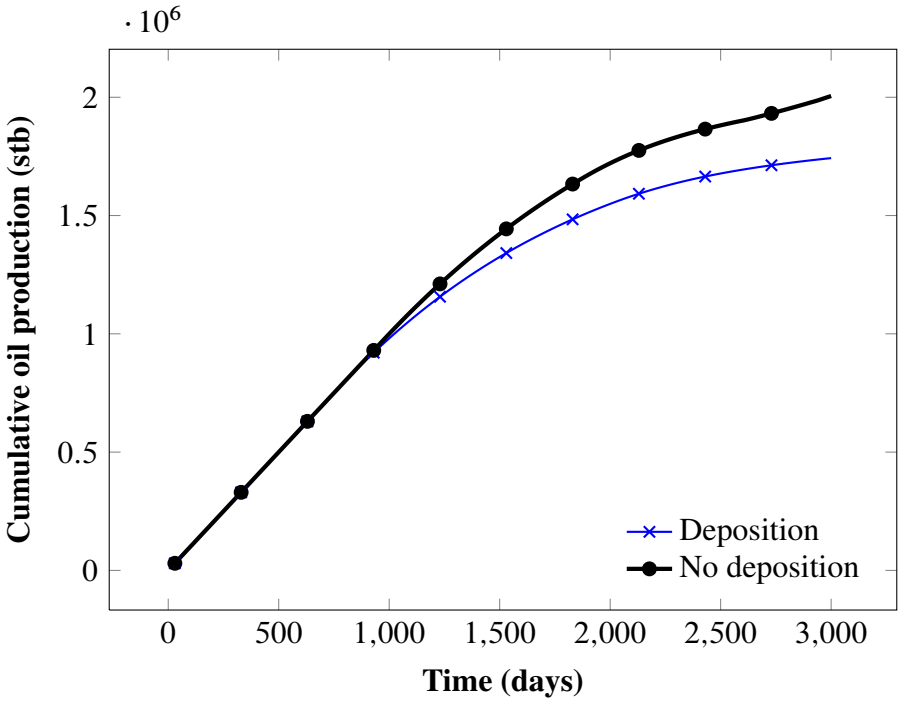

Fig. 6.9—Cumulative oil production after 3,000 days for a homogeneous reservoir modeled using two approaches: considering asphaltene precipitation, and neglecting it. It shows a difference of 13 in the results, which highlights the importance of including asphaltene in the analyses.

This parameter dictates how permeability changes as asphaltene deposits and reduces the pore volume. High values result in a linear and gentle slope. On the other hand, low values give a steep exponential decline. This flexibility allows the model to represent scenarios with different pore distribution and porosity-permeability relation. In addition, permeability reduction directly affects cumulative oil production, with reduction of up to 60% in the cases evaluated, as shown in **Fig. 6.11**.

6.2 Heterogeneous reservoir performance

A heterogeneous geologic model with asphaltene precipitation was analyzed in order to evaluate asphaltene behavior under more realistic conditions and test the robustness of the simulation code. The geology represents a simplified fluvial environment generated with

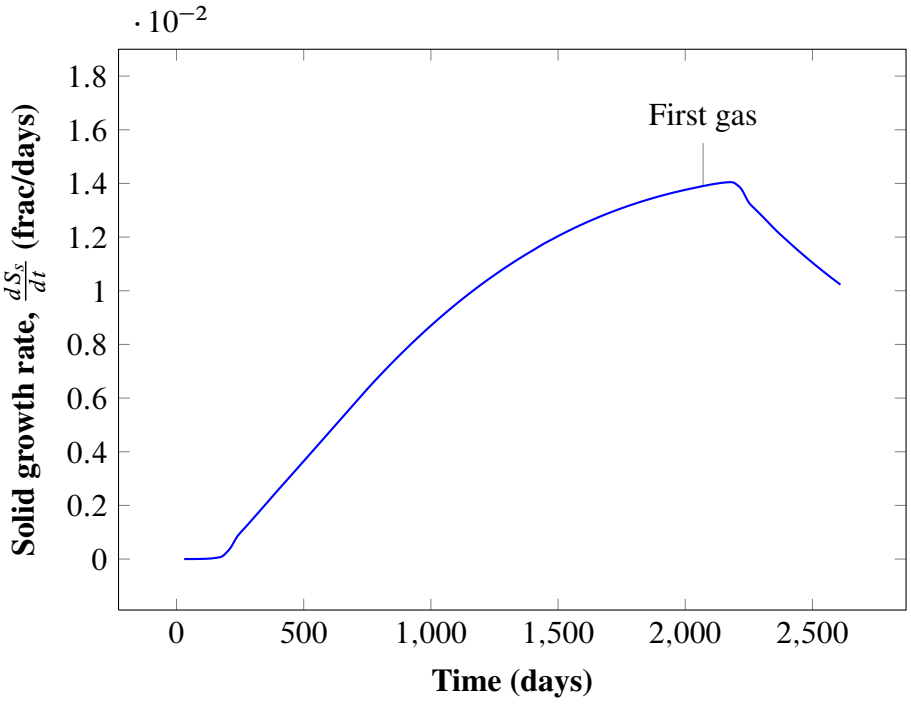

Fig. 6.10—The negative slope of the derivative of solid saturation with respect to time defines the beginning of stage 4.

the built-in stochastic algorithm found in PETREL®.

The adaptive channels were modeled using 15 channels and 2 facies (channel and levee sand). The layout and geometry of the deposition environment were defined using a triangular distribution, with 0°orientation. The average channel amplitude was set to 800 feet, with maximum and minimum values of 600 feet and 1,000 feet respectively. The wavelength defined the average distance between two consecutive channel turns, with an average value of 1,500 feet, 1,000 feet minimum, and 2,000 feet maximum. The channels contort is represented by the relative sinuosity parameter (Schlumberger, 2010) using an average of 0.3, minimum of 0.2, and maximum of 0.4 to produce braided channels. Each channel had an average width of 300 feet (150 feet minimum and 450 feet maximum), while the levee was on average 50% of the channel width (0.2 minimum and 0.7 maximum) with a roughness of 0.2.

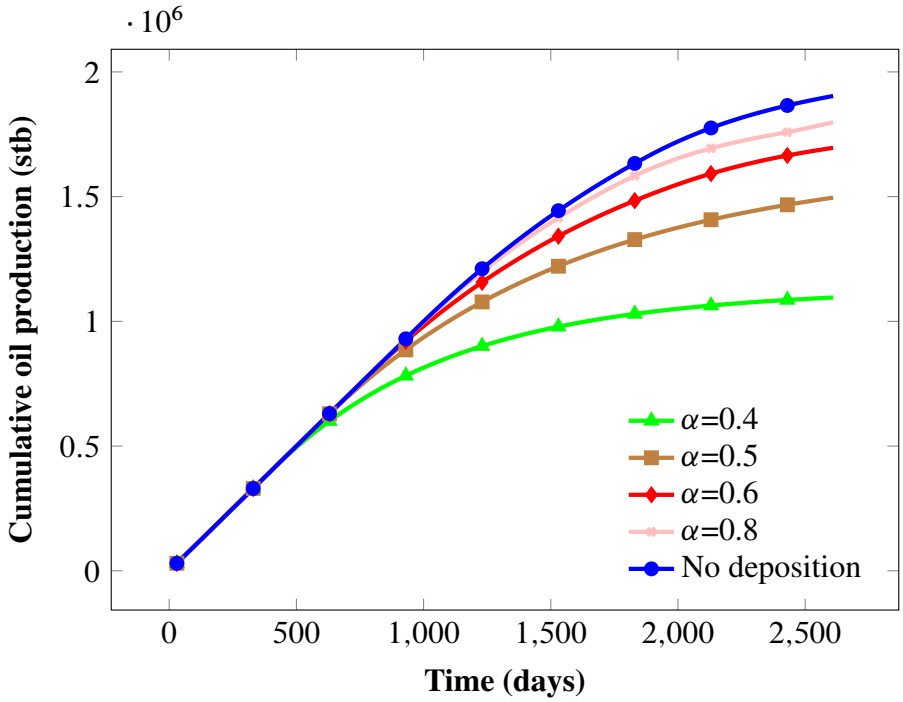

Fig. 6.11—Sensitivity analysis on the permeability reduction directly affects the cumulative oil production. The lower the α parameter, the highest the reduction of permeability and the lower the final oil recovery.

Using these parameters, the geologic model represented a channel-levee system. Each facies was assigned a single porosity and permeability value. The channel has a porosity of 16 %, and a horizontal permeability of 12 mD; the horizontal/vertical permeability ratio was maintained at 0.1. The levee sand had a porosity of 5 % with horizontal permeability of 0.1 mD. Permeability distribution is shown in **Fig. 6.12**. For the fluid and rock-fluid properties, we used the values described in the mechanistic analysis section. The well is located in the center of the model.

In the heterogeneous case, it is possible to identify the same precipitation stages as previously described for the homogeneous case. At 60 days, asphaltene begins to deposit near the wellbore where the lowest pressure is found (stage 2). Precipitation relates directly to pressure distribution, and for a heterogeneous system, it means that the zones with higher permeability will deplete faster and will experience first the effect of asphaltene precipita-

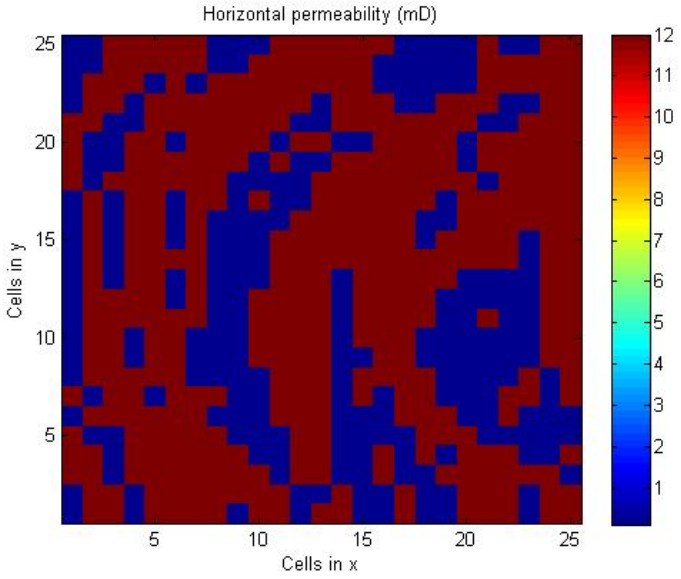

Fig. 6.12—Permeability distribution in the heterogeneous reservoir representing a fluvial depositional environment. Each facies was assigned a single permeability value.

tion, as shown in **Fig. 6.13**. The rest of the reservoir remains above the AOP.

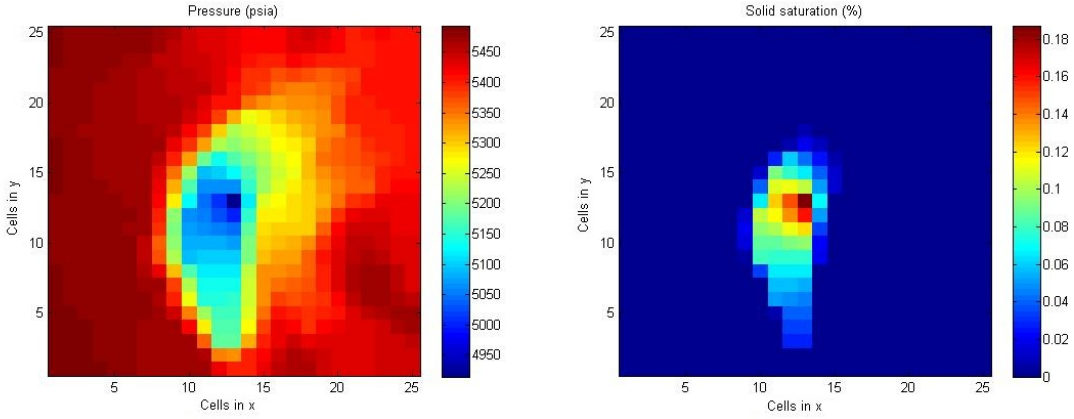

Fig. 6.13—Pressure distribution at 60 days (stage 2) for the heterogeneous reservoir shows asphaltene deposited in zones with high permeability, where the pressure depletes faster.

Stage 3 is observed at 600 days, when the pressure is reduced below the AOP along most of the reservoir. Pressure distribution is highly unequal due the high permeability contrast

between zones. Similar to the homogeneous case, the highest solid deposition is initially observed in the wellbore (**Fig. 6.14** for 600 days). However, at 900 days, the highest precipitation is observed in the wellbore vicinities (**Fig. 6.15**). At this point, we have not observed reduction of production compared to a case without asphaltene.

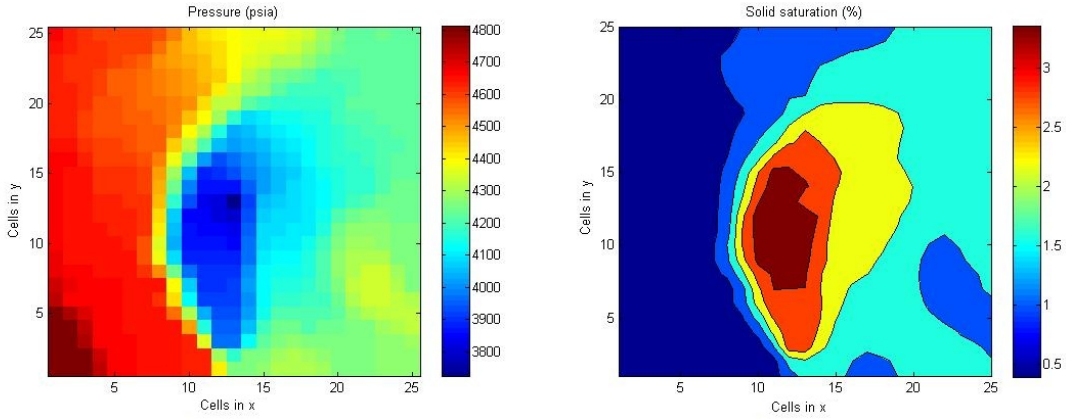

Fig. 6.14—Pressure distribution at 600 days (stage 3) for the heterogeneous reservoir shows the highest solid saturation near the wellbore.

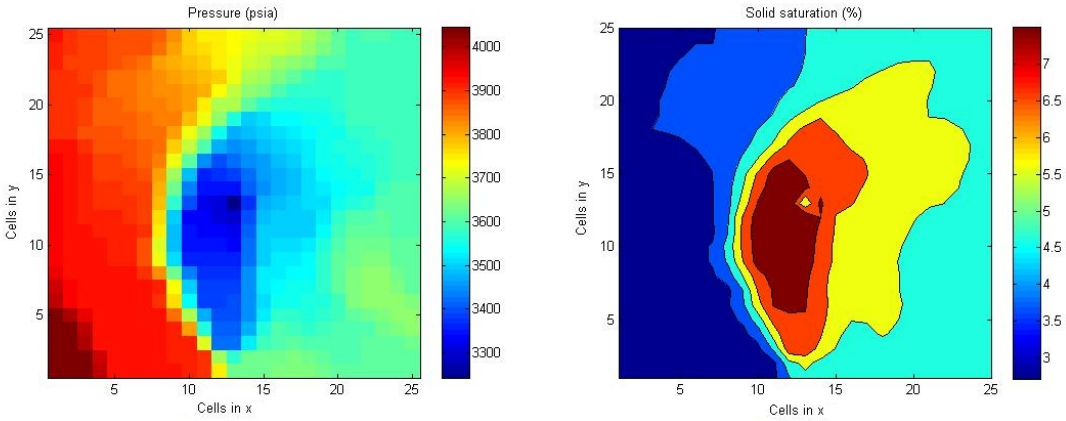

Fig. 6.15—Pressure distribution at 900 days (stage 3) for the heterogeneous reservoir shows the highest solid saturation near the wellbore.

For our case, the effect of asphaltene precipitation in the oil production occurs after 800 days of production, when oil production of the case that considers asphaltene precipitation

deviates from the case without considering asphaltene (**Fig. 6.16**).

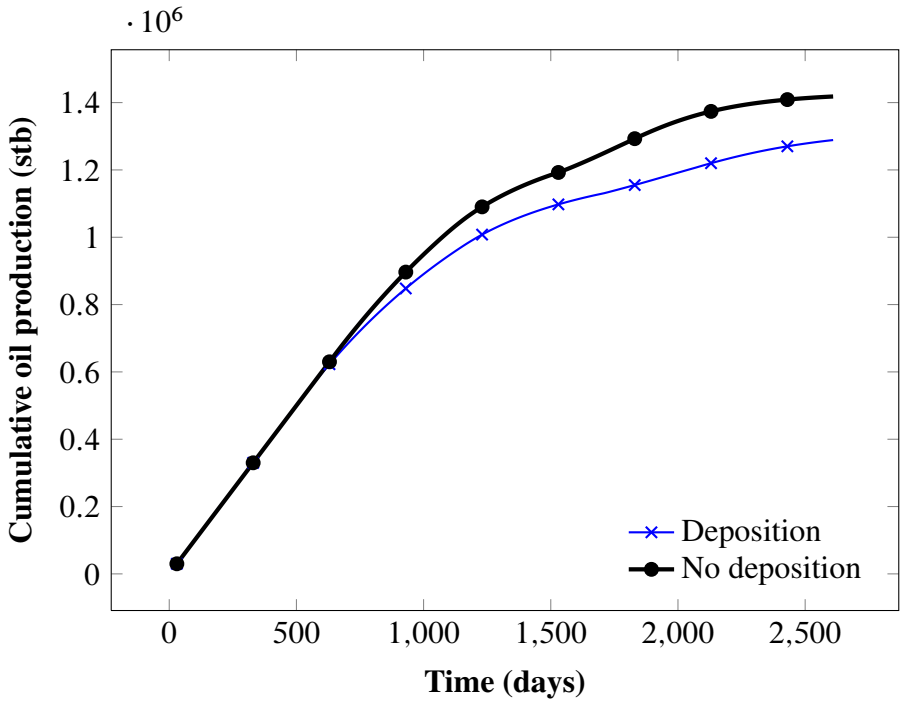

Fig. 6.16—Cumulative oil recovery for the heterogeneous case shows that after 800 days of production, the recovery considering asphaltene deviates from the ideal case where asphaltene is neglected.

Finally, stage 5 occurs when the rate of deposition is reduced, as shown in **Fig. 6.17** at 1,380 days. For the heterogeneous case, we observe a more gradual transition between the two stages. The high heterogeneity contrast result in multiple stages co-existing along the reservoir at the same time. Similar to the observations from the homogeneous case, the beginning of this phase is marked when the pressure reaches the bubble point pressure.

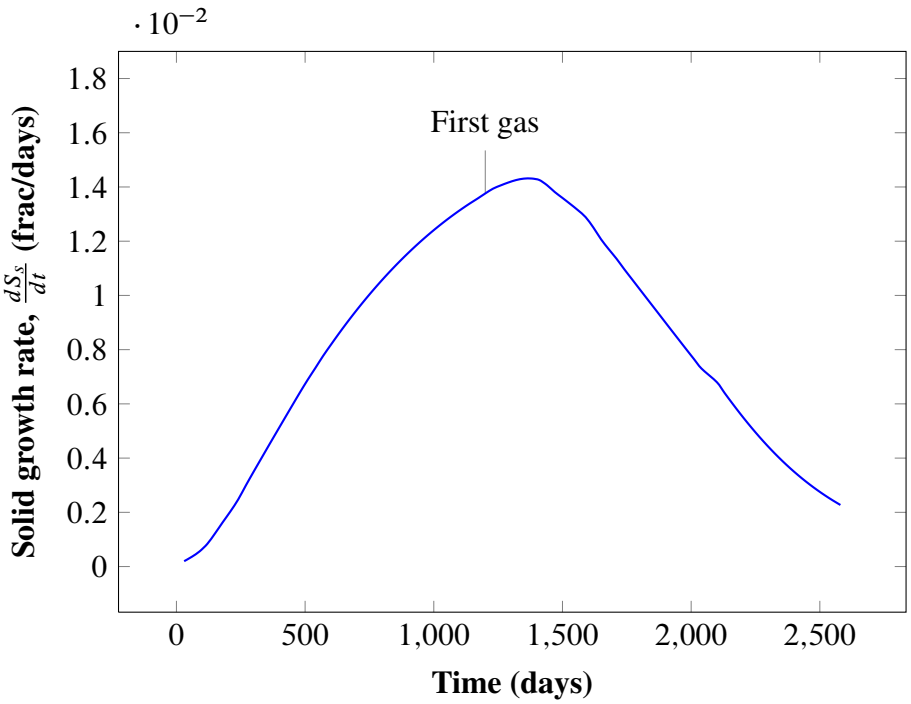

Fig. 6.17—The solid growth plot shows the change of slope representing the beginning of stage 5. For a heterogeneous case, the transition between stages is more gradual, compared to the homogeneous case, as the reservoir may exhibit multiple stages at the same time.

CHAPTER VII
CONCLUSIONS AND RECOMMENDATIONS

During the development of this research, we reached the following conclusions:

1. We proved the ability to model asphaltene behavior using a three-phase algorithm solved with Peng-Robinson equation of state and assuming asphaltene as a pure liquid-dense phase. This was validated by reproducing experimental data for cases with pressure depletion and solvent injection.

2. Results show a superior thermodynamic predictions compared to all previous techniques with fewer tunable parameters. It also has comparable cost to existing commercial models, taking only 1.1 more time to execute.

3. For the 45 cases analyzed, all of them characterized with 12 components, the execution time of the three-phase flash was in average 4.47 times slower compared to a conventional two-phase flash.

4. Sensitivity analyses on asphaltene properties indicated expected phase behavior when perturbing the characterization parameters. Asphaltene precipitation and bubble point pressure increases when incrementing critical pressure, critical temperature, acentric factor, or binary interaction coefficient between asphaltene and the lighter components of the mixture.

5. The IMPESC solution method allowed to represent the relationship between the fluid and the rock properties (porosity and permeability).

6. Reservoir with asphaltene precipitation exhibit four different stages depending on the fluid behavior and formation damage observed: pressure above the upper AOP, near wellbore pressure below upper AOP, reservoir pressure below the upper AOP, and reduced solid growth.

7. Formation damage due to asphaltene precipitation can be significant and can considerably affect the reservoir performance. A more reliable reservoir simulator that predicts the behavior of asphaltene is one of the most important techniques that we can use to develop a proper reservoir development strategy.

The proposed recommendation and future work related to this project are:

1. Using the reservoir simulator developed in this research, manage production strategies to mitigate asphaltene precipitation, including: CO_2 injection, pressure maintenance, etc.

2. Develop and implement a model for properly representing the physical mechanisms of flow of asphaltene in the pore throat.

3. Optimize computational time by analyzing the development of the asphaltene model using fully implicit methods.

4. Include the deposition of asphaltene in the wellbore and its effect on overall skin.

5. Include water phase and its interaction with precipitated asphaltene, including formation of emulsions, effect on viscosity and wettability, and transportation of precipitate.

REFERENCES

Acs, G., Doleschall, S., and Farkas, E. 1985.General purpose compositional model. *SPE Journal* **25**(4):543–553.

Burke, N. E., Hobbs, R. E., and Kashou, S. F. 1990.Measurement and modeling of asphaltene precipitation. *SPE Journal of Petroleum Technology* **42**(11):1440–1446.

Calsep 2010; PVTSim method documentation. Lyndgby, Denmark.

Cao, H. 2002.; Development of techniques for general purpose simulators. Ph.D. dissertation; Stanford University. Palo Alto, California.

Civan, F. 1992. Evaluation and comparison of the formation damage models. SPE 23787 presented at the SPE Formation Damage Control Symposium, 26-27 February 1992, Lafayette, Louisiana.

Civan, F. 2000.*Reservoir Formation Damage: Fundamentals, Modeling, Assessment, and Mitigation*. Gulf Publishing Company. Houston, Texas.

Coats, K. H. 1980.An equation of state compositional model. *SPE Journal* **20**(5):363–376.

Computer Modeling Group Ltd. 2011; Generalized equation-of-state model compositional reservoir simulator manual. Calgary, Alberta, Canada.

Fazelipour, W. 2007.; Development of a fully implicit, parallel, equation-of-state compositional simulator to model asphaltene precipitation in petroleum reservoirs. Ph.D. dissertation; The University of Texas at Austin. Austin, Texas.

Firoozabadi, A. 1999.*Thermodynamics of hydrocarbon reservoirs*. McGraw-Hill.

Fussell, L., and Fussell, D. 1979.An iterative technique for compositional reservoir models. *SPE Journal* **19**(4):211–220.

Gonzalez, D. L., Hirasaki, G. J., Creek, J., and Chapman, W. G. 2007.Modeling of asphaltene precipitation due to changes in composition using the perturbed chain statistical associating fluid theory equation of state. *Energy & Fuels* **21**(3):1231–1242.

Gruesbeck, C. R., C. 1982.Entrainment and deposition of fine particles in porous media. *SPE Journal* **22**(6):847–856.

Gupta, A. 1986.; A model for asphaltene flocculation using an equation of state. Ph.D. dissertation; The University of Calgary. Calgary, Canada.

Hirschberg, A., deJong, L., Schipper, B., and Meijer, J. 1984.Influence of temperature and pressure on asphaltene flocculation. *SPE Journal of Petroleum Technology* **24**(3):283–293.

Hunt, J., Winans, R., and Miller, J. 1997.*Characterization of asphaltene from processed resids*. Department of Energy. Naperville, Illinois.

Kontogeorgis, G. M., Michelsen, M. L., Folas, G. K., Derawi, S., von Solms, N., and Stenby, E. H. 2006.Ten years with the cpa (cubic-plus-association) equation of state. part 2. cross-associating and multicomponent systems. *Industrial & Engineering Chemistry Research* **45**(14):4869–4878.

Leontaritis, K., and Mansoori, G. 1987. Asphaltene flocculation during oil production and processing: A thermodynamic collodial model. SPE 16258 presented at the SPE International Symposium on Oilfield Chemistry, 4-6 February 1987, San Antonio, Texas.

Leontaritis, K. J. 1996.The asphaltene and wax deposition envelopes. *Fuel Science and Technology International* **14**(1-2):13–39.

Leontaritis, K. J., and Ali Mansoori, G. 1988.Asphaltene deposition: a survey of field experiences and research approaches. *Journal of Petroleum Science and Engineering* **1**(3):229–239.

Li, Z., and Firoozabadi, A. 2010a.Cubic-plus-association equation of state for asphaltene precipitation in live oils. *Energy Fuels* **24**(5):2956–2963.

Li, Z., and Firoozabadi, A. 2010b.Modeling asphaltene precipitation by n-alkanes from heavy oils and bitumens using cubic-plus-association equation of state. *Energy Fuels* **24**(2):1106–1113.

Liu, K. 1997.; New strategies and procedures for efficient compositional reservoir simulation. Ph.D. dissertation; Texas A & M University. College Station, Texas.

Lohrenz, J., Bray, B. G., and Clark, C. R. 1964.Calculating viscosities of reservoir fluids from their compositions. *Journal of Petroleum Science and Engineering* **16**(10):1171–1176.

Mansoori, J. 1982.Discussion of compositional modeling with an equation of state. *SPE Journal* **22**(2).

McCain, W. D. 1990.*The Properties of Petroleum Fluids*. PennWell Books. Tulsa, Oklahoma.

Michelsen, M., and Mollerup, J. 2007.*Thermodynamic models: fundamentals & computational aspects*. Tie-Line Publications. Holte, Denmark.

Nghiem, L. 1999.; Phase behavior modeling and compositional simulation of asphaltene deposition in reservoirs. Ph.D. dissertation; University of Alberta. Edmonton, Canada.

Nghiem, L., Fong, D., and Aziz, K. 1981.Compositional modeling with an equation of state. *SPE Journal* **21**(6).

Pan, H., and Firoozabadi, A. 2000.Thermodynamic micellization model for asphaltene precipitation from reservoir crudes at high pressures and temperatures. *SPE Production Operations* (1):58–65.

Peaceman, D. W. 1978.Interpretation of well-block pressures in numerical reservoir simulation. *SPE Journal* **18**(3):183–194.

Peaceman, D. W. 1983.Interpretation of well-block pressures in numerical reservoir simulation with nonsquare grid blocks and anisotropic permeability. *SPE Journal* **23**(3):531–543.

Pedersen, K., and Christensen, P. 2006.*Phase behavior of petroleum reservoir fluids*. CRC/Taylor & Francis. Boca Raton, Florida.

Peng, D.-Y., and Robinson, D. B. 1976.A new two-constant equation of state. *Industrial Engineering Chemistry Fundamentals* **15**(1):59–64.

Rachford, H., and Rice, J. 1952.Procedure for use of electronic digital computers in calculating flash vaporization hydrocarbon equilibrium. *Journal of Petroleum Technology* **4**(10).

Redlich, O., and Kwong, J. N. S. 1949.On the thermodynamics of solutions. v. an equation of state. fugacities of gaseous solutions. *Chemical Reviews* **44**(1):233–244.

Robinson, D., and Peng, D. 1978.*The Characterization of the Heptanes and Heavier Fractions for the GPA Peng-Robinson Programs*. University of Alberta, Edmonton, Alberta. Project. GPA Report RR-28.

Schlumberger 2010; Petrel seismic-to-simulation software help manual. Oslo, Norway.

Schlumberger 2011; Eclipse technical description and reference manual. Abingdon, United Kingdom.

Soave, G. 1972.Equilibrium constants from a modified Redlich-Kwong equation of state. *Chemical Engineering Science* **27**(6):1197–1203.

Spillette, A., Hillestad, J., and Stone, H. 1973. A high-stability sequential solution approach to reservoir simulation. This paper was prepared for the 48th Annual Fall Meet-

ing of the Society of Petroleum Engineers of AIME, to be held in Las Vegas, Nevada, Sept. 30-Oct. 3, 1973.

Thomas, F. B., Bennion, D., Bennion, D., and Hunter, B. 1992.Experimental and theoretical studies of solid precipitation from reservoir fluid. *J Can Petrol Technol* **31**:22–31.

Vafai, K. 2005.*Handbook of Porous Media*. CRC Press. New York, New York.

Valbuena, E. 2011.; Analytical estimation of CO2 storage capacity in depleted oil and gas reservoirs based on thermodynamic state functions. Master's thesis; Texas A&M University. College Station, Texas.

Vargas, F. M., Gonzalez, D. L., Hirasaki, G. J., and Chapman, W. G. 2009.Modeling asphaltene phase behavior in crude oil systems using the perturbed chain form of the statistical associating fluid theory (pc-saft) equation of state. *Energy Fuels* **23**:11401146.

van der Waals, J. 1873.; Over de continuiteit van den gas - en vloeistoftoestand (on the continuity of the gas and liquid state). Ph.D. dissertation; Leiden University. Leiden, The Netherlands.

Wang, S. 2000.; Simulation of asphaltene deposition in petroleum reservoirs during primary oil recovery. Ph.D. dissertation; University of Oklahoma. Norman, Oklahoma.

Watts, J. 1986.A compositional formulation of the pressure and saturation equations. *SPE Reservoir Engineering* (3):243–252.

Wilson, G. 1969. A modified redlich-kwong equation of state, application to general physical data calculation. Paper No. 15C presented at the 1969 AIChE 65th National Meeting, Cleveland, Ohio, March 4-7, 1969.

Yan, W., Michelsen, M., and Stenby, E. 2011. On application of non-cubic eos to compositional reservoir simulation. SPE 142955 presented at the SPE EUROPEC/EAGE Annual Conference and Exhibition, 23-26 May 2011, Vienna, Austria.

Yi, T., Fadili, A., Ibrahim, M. N., and Al-Matar, B. S. 2009. Modeling the effect of asphaltene on the development of the marrat field. SPE 120988 presented at the 8th European Formation Damage Conference, 27-29 May 2009, Scheveningen, The Netherlands.

Young, L. C., and Stephenson, R. E. 1983.A generalized compositional approach for reservoir simulation. *SPE Journal* (5):727–742.

APPENDIX A

DERIVATION OF PARTIAL MOLAR VOLUME

The change of total volume with respect to the change of moles of component i at constant pressure and temperature is defined as the partial molar volume (Eq. A.1). It represents the contribution of component i to the overall volume of the mixture.

$$\overline{V}_i = \left(\frac{\partial V_t}{\partial n_i}\right)_{p,T,n_j} \tag{A.1}$$

Valbuena (2011) proposed the concept of Generalized Partial Molar Volume (PMV) describing Eq. A.1, which can be applied for multiple component changing its molar fraction. It shows that if two of the three variables are related, then one of the variables may be selected as the independent variable and the other two as dependent variables (Michelsen and Mollerup, 2007).

$$F(p, V_t, T, n) = 0 \tag{A.2}$$

If n is kept constant, we can work the partial derivative expressions, we can apply the "minus one rule", resulting in Eq. A.3.

$$\left(\frac{\partial p}{\partial V_t}\right)_{T,n}\left(\frac{\partial V_t}{\partial T}\right)_{p,n}\left(\frac{\partial T}{\partial p}\right)_{V_t,n} = -1 \tag{A.3}$$

In oil and gas reservoirs, temperature is assumed to remain constant. Eq. A.4 represents the relationship between the variables.

$$\left(\frac{\partial p}{\partial V_t}\right)_{T,n}\left(\frac{\partial V_t}{\partial n_i}\right)_{p,T,n_j}\left(\frac{\partial n_i}{\partial p}\right)_{V_t,T,n_j} = -1 \tag{A.4}$$

From Eq. A.4 we can define the partial molar volume as shown in Eq. A.5.

$$\overline{V}_i = \left(\frac{\partial V_t}{\partial n_i}\right)_{p,T,n_j} = -\frac{\left(\frac{\partial p}{\partial n_i}\right)_{V_t,T,n_j}}{\left(\frac{\partial p}{\partial V_t}\right)_{T,n}} \tag{A.5}$$

To derive Eq. A.5 we use the pressure equation as defined by Peng-Robinson. Re-writting Eq. 3.12 as a function of total fluid volume V_t results in Eq. A.6. The following section derives the pressure equation with respect to V_t and n_i

$$p = \frac{RTn}{V_t - nb} - \frac{n^2 a(T)}{V_t^2 + 2nbV_t - n^2b^2} \tag{A.6}$$

Partial derivative of p with respect to V_t

After differentiating Eq. A.6 with respect to total volume, we obtained Eq. A.7, where the parameters $a(T)$ and b are independent from the total volume of the mixture.

$$\left(\frac{\partial p}{\partial V_t}\right)_{T,\vec{N}} = -\frac{RTn}{(V_t - nb)^2} + \frac{2n^2 a(T)(V_t + nb)}{(V_t^2 + 2nbV_t - n^2b^2)^2} \tag{A.7}$$

Partial derivative of p with respect to n_i

Eq. A.6 will be derived in two parts: repulsion and attraction.

$$p = \underbrace{\frac{RTn}{V_t - nb}}_{Repulsion} - \underbrace{\frac{n^2 a(T)}{V_t^2 + 2nbV_t - n^2b^2}}_{Attraction} \tag{A.8}$$

Repulsion Term Derivative

$$\frac{\partial}{\partial n_i}\left(\frac{RTn}{V_t - nb}\right)_{V_t,T,n_j} = \frac{RT}{(V_t - nb)^2}\left[(V_t - nb) - \frac{\partial}{\partial n_i}(V - nb)\right] \tag{A.9}$$

Applying linear mixing rules, described in Section A.4:

$$\begin{aligned}\frac{\partial}{\partial n_i}\left(\frac{RTn}{V_t - nb}\right)_{V_t,T,n_j} &= \frac{RT}{(V_t - nb)^2}\left[(V_t - nb) + nb_i\right] \\ &= \frac{RT}{V_t - nb} + \frac{RTnb_i}{(V_t - nb)^2}\end{aligned} \tag{A.10}$$

Attraction Term Derivative

$$\begin{aligned}\frac{\partial}{\partial n_i}\left(\frac{n^2 a(T)}{V_t^2 + 2nbV_t - n^2b^2}\right)_{V_t,T,n_j} &= \frac{1}{D^2}\left\{D\left[n^2\frac{\partial a(T)}{\partial n_i} + 2na(T)\right]\right. \\ &- a(T)n^2\left[2V_t\left(n\frac{\partial b}{\partial n_i} + b\frac{\partial n}{\partial n_i}\right)\right. \\ &- \left.\left.\left(n^2\frac{\partial b^2}{\partial n_i} + b^2\frac{\partial n^2}{\partial n_i}\right)\right]\right\}\end{aligned} \tag{A.11}$$

Where D is given by Eq. A.12

$$D = V_t^2 + 2nbV_t - n^2b^2 \tag{A.12}$$

Applying the quadratic mixing rule, described in Section A.4:

$$\frac{\partial}{\partial n_i}\left(\frac{n^2 a(T)}{D}\right)_{V_t,T,n_j} = \frac{1}{D^2}\left[D\,(2n\Psi) - a(T)n^2\,(2V_t b_i - 2nbb_i)\right] \tag{A.13}$$

Where Ψ is a part of the partial derivative term of $a(T)$ with respect to n_i. as shown in Eq. A.14.

$$\Psi = \sum_{j \neq i=1}^{Nc} \left[x_j \left(a\alpha_{ij} \right) \right] + x_i a_i \alpha_i \tag{A.14}$$

Simplifying Eq. A.13, we have

$$\frac{\partial}{\partial n_i} \left(\frac{n^2 a(T)}{D} \right)_{V_t, T, n_j} = \frac{2n\Psi}{D} - \frac{2n^2 a(T) V_t b_i}{D^2} + \frac{2n^3 a(T) b b_i}{D^2} \tag{A.15}$$

Finally, combining the repulsion (Eq. A.10) and the attraction term (Eq. A.13), we have the derivative of p with respect to n_i shown in Eq. A.16.

$$\begin{aligned} \left(\frac{\partial p}{\partial n_i} \right)_{V_t, T, n_j} &= \frac{RT}{V_t - nb} + \frac{RTnb_i}{(V_t - nb)^2} - \frac{2n\Psi}{D} \\ &+ \frac{2n^2 a(T) V_t b_i}{D^2} - \frac{2n^3 a(T) b b_i}{D^2} \end{aligned} \tag{A.16}$$

Final partial molar volume form

Combining the partial derivative of p with respect to V_t and the partial derivative of p with respect to n_i, we obtain the final form for partial molar volume (Eq. A.17).

$$\overline{V}_i = -\frac{R_1 + A_1}{D_1} \tag{A.17}$$

Where:

$$R_1 = \frac{RT}{v - b} + \frac{RTb_i}{(v - b)^2} \tag{A.18}$$

$$A_1 = -\frac{2\Psi}{D_v} + \frac{2a(T) v b_i}{(D_v)^2} - \frac{2a(T) b b_i}{(D_v)^2} \tag{A.19}$$

$$D_1 = -\frac{RT}{(v-b)^2} + \frac{2a(T)(v+b)}{(D_v)^2} \tag{A.20}$$

Where D_v is:

$$D_v = V_m^2 + 2bV_m - b^2 \tag{A.21}$$

Mixing rules

This section shows the mixing rules used in the differentiation of the partial molar volume.

Linear mixing rule

For a mixture of N_c components, we define the b parameter as:

$$b = \sum_{i=1}^{Nc} x_i b_i \tag{A.22}$$

We can express Eq. A.22 in terms of moles:

$$b = \sum_{i=1}^{Nc} \frac{n_i}{n} b_i \tag{A.23}$$

Differentiating Eq. A.23 with respect to n_i, we have:

$$\frac{\partial b}{\partial n_i} = \sum_{i=1}^{Nc} \frac{b_i}{n^2} \left(n \frac{\partial n_i}{\partial n_i} - n_i \frac{\partial n}{\partial n_i} \right) \tag{A.24}$$

Expressing Eq. A.24 in terms of liquid mole fraction:

$$\frac{\partial b}{\partial n_i} = \frac{1}{n} (b_i - b) \tag{A.25}$$

Quadratic mixing rule

For a 3-component mixture, the parameter $a(T)$ is represented by the following quadratic rule:

$$\begin{aligned} a(T) &= 2x_1x_2(a\alpha_{1,2}) + 2x_2x_3(a\alpha_{2,3}) + 2x_1x_3(a\alpha_{1,3}) \\ &+ x_1^2a_1\alpha_1 + x_2^2a_2\alpha_2 + x_3^2a_3\alpha_3 \end{aligned} \tag{A.26}$$

Where $a\alpha_{i,j}$ is:

$$a\alpha_{i,j} = \sqrt{a_i\alpha_i a_j\alpha_j}\left(1 - k_{i,j}\right) \tag{A.27}$$

Expressing Eq. A.26 as a function of number of moles, we have:

$$\begin{aligned} a(T) &= \frac{1}{n^2}\Big[2n_1n_2(a\alpha_{1,2}) + 2n_2n_3(a\alpha_{2,3}) + 2n_1n_3(a\alpha_{1,3}) \\ &+ n_1^2a_1\alpha_1 + n_2^2a_2\alpha_2 + n_3^2a_3\alpha_3\Big] \end{aligned} \tag{A.28}$$

Differentiating Eq. A.28 with respect to the number of moles, we have:

$$\frac{\partial a(T)}{\partial n_1} = -\frac{2}{n^3}\Lambda + \frac{1}{n^2}\left[2n_2(a\alpha_{1,2}) + 2n_3a\alpha_{1,3} + 2n_1a_1\alpha_1\right] \tag{A.29}$$

Where Λ is:

$$\begin{aligned} \Lambda &= 2n_1n_2(a\alpha_{1,2}) + 2n_2n_3(a\alpha_{2,3}) + 2n_1n_3(a\alpha_{1,3}) \\ &+ n_1^2a_1\alpha_1 + n_2^2a_2\alpha_2 + n_3^2a_3\alpha_3 \end{aligned} \tag{A.30}$$

Generalizing the partial derivative of Eq. A.29 for N_c components, we have:

$$\frac{\partial a(T)}{\partial n_i} = \frac{2}{n}\left[\Psi - a(T)\right] \tag{A.31}$$

Where:

$$\Psi = \sum_{j \neq i=1}^{Nc} \left[x_j \left(a\alpha_{ij}\right)\right] + x_i a_i \alpha_i \tag{A.32}$$